Reviewer 1

Reviewer 1: Page 1 - Title: Suggest making it sharper. Delete 'understanding' and 'sensing' from 'Understanding Mn-nodule distribution and related deep-sea mining impacts using AUV-based hydroacoustic sensing and optical observations'.
Authors Comment: Title has been changed (DC).
Document Changes: Understanding Mn-nodule distribution and evaluation of related deep-sea mining impacts using AUV-based hydroacoustic and optical data.

R1: Page 4 – Study area (line 28-29): Introduce a map showing general location of the study area with latitude, longitude and depth contours to give a general perspective to the reader (these details are not required for the subsequent figures given in the manuscript).
AC: We added the coordinates for the center of the working area in Figure caption Figure 2.
DC: Black squares mark the study area (center 117°1 W 11°51N) shown in Figure 3.

R1: Page 8 – AUV based bathymetry . . ..abundance (line 7) : The word 'abundance' signifies 'quantity of resource per unit area (Kg/sqm)' whereas here the nodule occurrence is expressed in 'percentage'. So 'abundance' should be replaced with 'coverage'.
AC: Has been corrected.

R1: Page 8 – Large-scale variability (line 24) : The term 'large-scale variability' is misleading and suggest that it can be replaced with 'Macrotopographic variability'.
AC: It has been replaced (DC) to make this clearer.
DC: Broad scale variability (less detailed, correlation with ship-based bathymetric data, resolution 100-1000m)

R1: Page 10 – Fig. 5D : Mean size of nodule is given as 6.7 cm2, 15cm2, 17.4 cm2. 'Mean size' should be replaced with 'Mean area' as size cannot be expressed as square.
AC: To our understanding cm^2 can be used as an expression for size and we consider it as more suitable here than the expression "Mean-area"; of course, we are aware of buried areas of the nodules.

R1: Page 11 – Small-scale variability (line 21) : The term 'small-scale variability' is misleading and suggest that it can be replaced with 'Microtopographic variability'.
AC: Has been corrected (DC).
DC: Local scale variability (more detailed, correlation with AUV-based bathymetric data, resolution 1-100m)

R1: Page 17 – Broad-scale correlation. . ... (line 18) : Use of the term 'Broad scale . . .' is confusing and may be replaced with 'Regional scale. . ..' as it covers large area.
AC: Has been replaced as suggested.

R1: Page 17 - lines 25-28: Comment – Regional differences in nodule exposure (burial) could also be reason for this as nodules in Central Indian Ocean appear smaller due to more sediment cover as compared to those in the Pacific which could be due to differences in current velocities that influence settling of sediments.

AC: This should indeed be mentioned here and has been added to the text p.24, edited manuscript.

DC: Varying considerations of scale and regional differences in nodule exposure between different oceans across different studies have thus led to partly contradicting statements of the relationship between the Mn-nodule coverage/size and bathymetric settings.

R1: Page 19 – Broad vs small scale : In cartography 'large (broad) scale' means representing small distances (area) and 'small scale' means covering larger distances (areas) for a given unit. To avoid any confusion for the reader, suggest that authors clarify the meaning of 'large scale' and 'small scale' or make necessary corrections (for example use the terms such as 'regional' and 'local').

AC: This remark has been taken into account. We changed the passages through the text to avoid any confusion.

R1: Page 19-22 – Sediment plume resettling : This section is too long and without any breaks, so difficult to follow. Suggest that it could be divided into sub-sections with individual heading if possible and/or with paragraphs.

AC: Paragraphs and sub-sections have been added in the section (see manuscript, section 4.3).

R1: Page 22 - Conclusions – line 17: Start new para from 'With respect to. . ..'

AC: Has been changed as suggested.

Technical / editorial comments:

R1: At a few places where it is not clear, a question (?) mark is inserted in the text where the authors can make necessary corrections / additions as required.

AC: Thank you for the remarks. We made a number of additions/corrections at those places (see manuscript, changes are tracked).

AC: p.5, line 4-5: In these lines only the Experiments and year of conduction are named, not any references. MMAJ: BIE conducted in 1997 within the area of the Marcus-Wake Seamounts in the North Pacific Ocean. Reference: Yamada and Yamazaki, 1998;

R1: A few general editorial corrections required are as follows:
i. Apply superscript for '2 (square)' wherever required

AC: Has been corrected.

R1: ii. All references should be in bracket / parenthesis including author and year eg. (Page 2 – line 7 : Purser et al. 2016; Vanreusel et al. 2016).

AC: The citing format is one accepted format of the journal. But since it was commented from all other reviewers as well it has been changed to the suggested format.

R1: iii. Shipbased and AUV based may be replaced with ship-borne and AUV-borne

AC: We would like to stick with AUV-based and ship-based as this is a typical way to indicate with which platform the data have been acquired.

Cited References:

Yamada, H., and T. Yamazaki. 1998. "Japan's Ocean Test of the Nodule Mining System." 1998/1/1/.

Reviewer 2

1 General Comments

Reviewer 2: The authors of this study should present information on the mean nodule size …

Authors Comment: Considering the potential inaccuracy of nodule detection and separation of the image analysis tool, the application of quantiles on the size distribution allows a more accurate interpretation of the data (Peukert, 2016). Therefore, a mean size value would not be appropriate here. An explanation was added to the Appendix (see DC).

Document Changes: <u>Interpretation of Mn-nodule size results</u>

Considering the probable error in correctly detecting nodules by the image-analyzing tool, the application of quantiles of the size distribution allows a better interpretation of the data. It is suggested not to use size values of the smallest and largest 1 % of the quantile calculation, due to the above mentioned error source. The graph in figure A1 illustrates the quantiles of the calculated sizes of two images, which clearly differ from each other. The graph correctly displays a size difference between both images, indicating larger nodules for image #29302. This shows that the tool can be reasonably applied to calculate the nodule size. The best differentiation however exists for the 50% - 75% quantile. Towards larger and smaller size values the curves approach each other which points towards the detection of similar – non nodule - features in both images. Therefore, the median values are considered to best represent nodule size differences between images/areas. Since truly correct nodule identification by the tool cannot be ensured for this quantile, size values should not be seen and used as absolute values, but rather indicators of changes between areas that are compared.
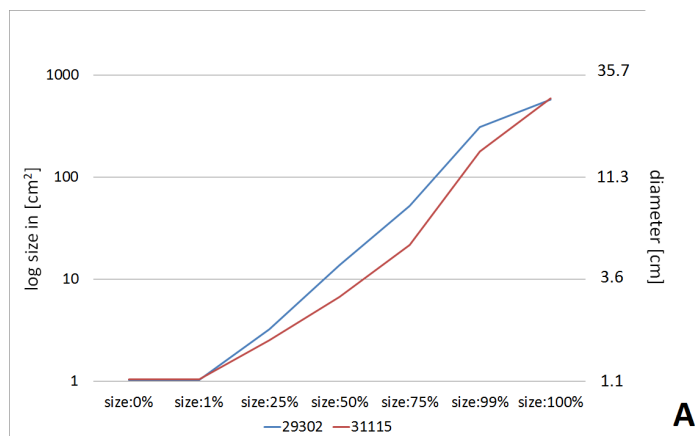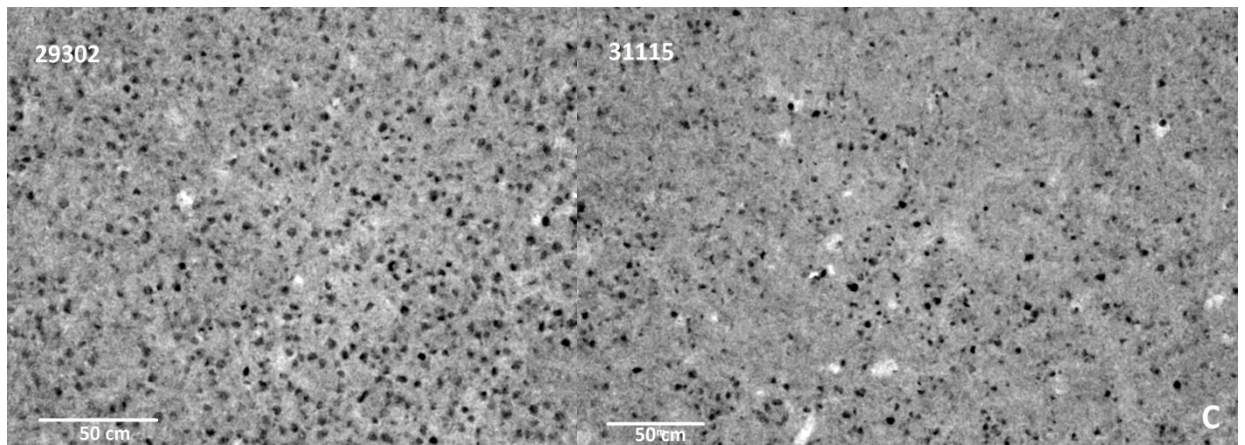
Figure A1: Two example images which clearly differ in nodule size and coverage. Graph A shows the calculated quantiles of Mn-nodule sizes in two example images (B, C).The results indicate that the strongest difference can be seen between the 50 and 75 % quantile.

R2: Moreover, Kuhn & Rathke (2017) showed in their study that a good correlation can be established between coverage data from box corer stations and image analysis for small-sized nodules […].The authors of this study […] should provide information if they have found a similar correlation. […]In the presented manuscript there is no information about precision and accuracy of the image analysis approach but this information is necessary and must be included.

AC: Indeed it would have been nice to correlate box-core data with image data. Unfortunately, we do not have corresponding image and box-core information. To do this properly, the seafloor photographs from before the sampling would be required, exactly knowing where the box-corer will take the sample. Alternatively, the AUV could have made a photo survey before and after the sampling. We do not have such data and thus cannot accommodate the request of the reviewer.

R2: […] Even if I doubt the absolute number of 12.5 % nodule coverage as the threshold value…

AC: The 12.5% Mn nodule coverage is of course not an absolute value, as it has been discussed several times. The calculated coverage results are in a range between 7-24%. However, the majority of 99% is between 8 and 17 %. Values below and above are outliers and can be considered as inaccuracy of the automatic nodule detection by "unusual" objects in the image (like tracks or a fish for example). 12.5% was set as a threshold, since it is the median and mean of this majority and is the highest occurring coverage amount (Figure 1, this comment section). Furthermore, applying this threshold, the difference in Mn nodule coverage follows bathymetric structures (especially in A2); of course, the differences in Mn nodule coverage are very low (and probably not relevant for resource assessment, which is not the goal of this study) but so are the morphological undulations within the studied area. To make this clearer, an explanation of the threshold value was added to the text (see DC, p.12, line 17ff.).

DC: Based on the automated image analyses, the majority of the seafloor shows nodule coverage values between 8% and 17% (Figure 5A). Values below and above this range (<1%) are to neglect, since they are caused by "unusual" objects (like tracks or organisms) in the images. In the following examinations the threshold between 'low' and 'high' Mn-nodule coverage is set at 12.5%; which is the analyzed mean coverage value of the considered range. In the eastern A2 sub-area a greater proportion of higher coverage values (13-16%) can be observed.
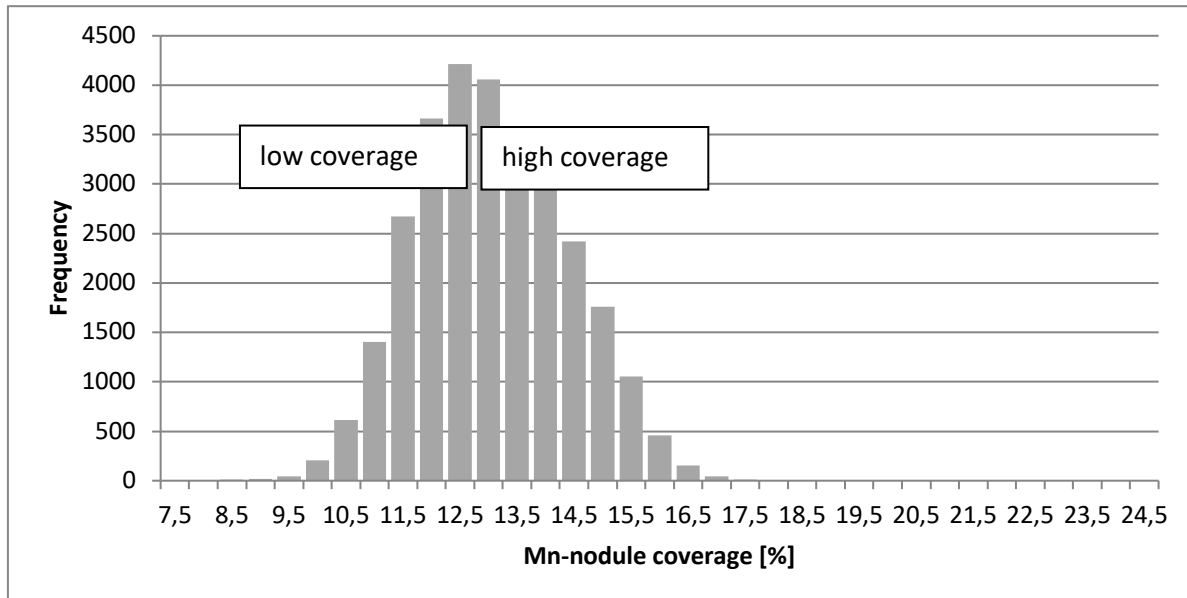
Figure 1: Frequency of Mn-nodule coverage results of the entire AUV photo survey Abyss 168. Mean value 13%.

R2: However, more real ground truth data from box corer stations would be necessary to verify the threshold value.

AC: That is true and would be part of further investigations, as mentioned above. The following sentence has been changed to mention this: section 4.1. p.24, line 4-5

DC: For absolute accurate resource assessments and verification of the results, detailed sampling based on this study would need to follow.

R2: I also wonder if there are any correlations between AUV-based backscatter data (such as BS intensity) and nodule coverage?

AC: Unfortunately, the BS data of the area analyzed in this study were not usable due to technical errors. The data from other areas though look very promising. These are part of other studies, which are currently in preparation.

R2: Another approach would be to analyze the nodule coverage and the hydroacoustic data based on artificial neural networks or on random forest. Did the authors try these approaches?

AC: This approach is part of other studies and was not pursued here. As mentioned above, the data used for this study were "data of opportunity" and not acquired to perform statistically correct machine learning approaches aiming at extrapolation of nodule coverage / resource assessments.

R2: What the manuscript generally lacks is real ground-truth data for Mn nodule coverage which can only be obtained from sampling with box corers. Is there any such information from the working area, e.g. from other cruises? I know that the BGR has carried out several expeditions to this area within their exploration campaign.

AC: As already mentioned above, box core sampling would be the next step based on these results for verification. This would require highly detailed sampling at exactly the same area analyzed here. In the publication of Kuhn et al. (2016), the box core stations are too far away (at least 500m) and also the BGR BC stations are located within this area, are too far away (Figure 2, this reviewer section). Thus, this data cannot be used as ground truth validation of our results. However, two

tracks of visual observations, which were also carried out from BGR, match more or less the AUV photo track of this area and provide similar observations (Peukert, 2016).
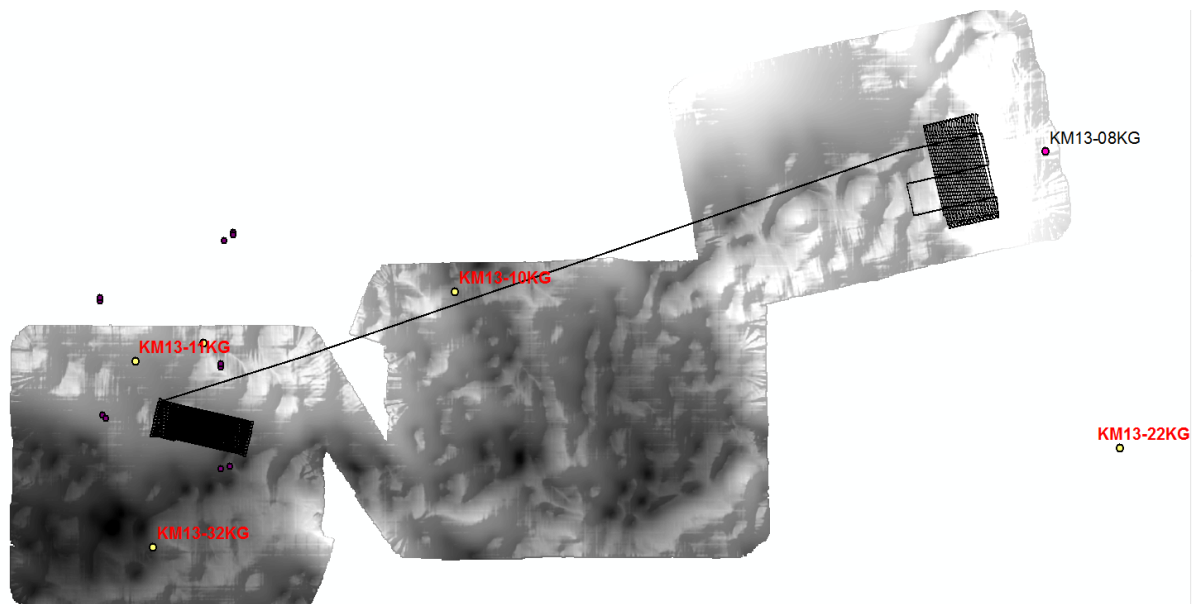

Figure 2: Box core stations marked as colored dots conducted by BGR within the study area.

2. Specific Comments

Abstract

R2: First sentence: Optical imaging data are no real ground truth data. If they could be linked with nodule coverage/abundance from box corer stations of this area, then one could speak of "ground-truth data". Otherwise, the authors should change this sentence removing the word "ground-truth".
AC: "Ground-truth" here means the visually from the AUV images detectable nodule coverage on the sediment surface, not the absolute coverage including the buried nodules. The term "ground-truth" seems reasonable to us for this study.

Nodule coverage vs. nodule abundance

R2: The authors sometimes use the term "nodule abundance" and sometimes "nodule coverage". There is a significant difference between both: abundance means the mass of nodules per area (e.g., in kg/m²) and coverage means the seafloor areal fraction covered by nodules in %. From image analysis only the coverage can be detected and this is what the authors mean in their manuscript (e.g. refer to Fig. 5). Therefore, the authors should only use the term "nodule coverage" in the manuscript.
AC: Thank you for this remark. We changed this throughout the text.

R2: [...] To my understanding this discrepancy is the main reason for the poor correlation coefficients and it may be caused by the observation that nodules are covered by sediments to a variable degree. But in images only the part of the nodules not covered by sediments can be analyzed and this may lead to a significant underestimation in both coverage and size of nodules as we can see it in the data presented in this manuscript.
AC: We are aware of the discrepancy between the visually detectable sediment surface and the "real" nodule coverage on the seafloor which is discussed in the paper (e.g. p.17, line 2ff. or p. 18,

lines 27-29). The results of Kuhn & Rathke (2017) regarding the accuracy is taken into account and mentioned in the text (section 4.1, p.24, l.4), see DC). This study aimed to show possible correlations between morphology on different scales and small-scale relative (not absolute!) changes in nodule coverage; such small scale-changes of course require very detailed sampling which needs to be taken out to verify the results as a next step. However, as mentioned in the paper, for habitat mapping purposes, nodules are considered as a hard substrate habitat where only the unburied part of the nodules on the sediment surface is relevant, making the visual mapping technique a very useful tool (p. 2, line 8-9, p. 17, line 4-6).

DC: Photographs only provide information of the sediment surface and thus will not be able to detect buried/sediment-covered Mn-nodules (Sharma and Kodagali, 1993; Sharma et al., 2010, 2013), resulting in an underestimation of the absolute Mn nodule coverage (Kuhn and Rathke, 2017).

Pit Structures

R2: The occurrence of pit structures may not only be restricted to larger depressions as stated on page 8, line 12, but could also be controlled by E-W trending linear structures as Fig. 4C may suggest.
AC: Yes, they could be controlled by E-W trending linear structures, however the AUV-mapped area does not allow the statement that E-W structures are more important than 'negative BPI' in general.

R2: A pit structure was sampled during SO140 with a box corer (station 107KG). There were no nodules on the sediment surface but two nodule layers at greater sediment depth (16 and 32 cm below surface; Kuhn et al., 2015). This contradicts the interpretation of the authors of this study of how larger nodules in the pit structure could have formed (page 18, line 20/21). […]
AC: We believe the reviewer considered larger structures in the SO140 cruise than the pits in focus of this study: "sizes from several tens of meters to 150m in diameter with a maximum depth of 4m" (p.8,line 11). However, at this point the reviewer mixes this study's "depressions" which are proposed to contain higher nodule coverages with this study's "pits", where no nodules can be seen at the sediment surface. We argue that nodules could be buried here (p.27, line 4-5, see edited manuscript), which is in agreement with your findings.

R2: […]BGR data suggest that larger nodules have a larger diagenetic fraction and thus should have grown faster. A larger diagenetic fraction, however, is only possible at sites with higher sedimentation rates and/or higher TOC content. A slightly higher sedimentation rate in areas of higher nodule coverage is also discussed by the authors of this study further down in the manuscript (page 18, line 30/31). Moreover, the pit structures are interpreted as sites of higher sedimentation rates (page 18, lines 35ff.). Why should other depressional sites behave differently in terms of the sedimentation regime?
AC: We distinguish between "depressions" and "pits", which occur within wider depressions (section 3.1, p. 12, line 9-11). In section 4.2.2. where the lack of Mn nodule coverages in these structures are discussed, we changed the text so the difference becomes more prominent (see DC).
DC: p. 26, line 29ff (see edited manuscript): Rather special for the presented data set are the pronounced pit structures, observed throughout the AUV-mapped area with very little to no Mn-nodules observed at the sediment surface, which is in contradiction to the wider depressions, where higher Mn-nodule coverage was observed.

AC: Our interpretation is that only in the pits the sedimentation rate is too high for nodules to appear at the sediment surface (because they were buried, p.18, lines 32-34), which is in agreement with the

reviewer's above mentioned findings. The pits are likely to be younger structures; nodules have formed within the depressions first. The collapse forming the pits occurred later. The nodules within the pits were then buried by sediments following the gravity to the deepest point and accumulating there.

We added the interpretation of pits being marine karsts and the associated reference to the interpretations (see DC).

DC: p. 27, lines 5-7 (edited manuscript): The formation process of the pits is unclear, but could be karst structures, as proposed by Kuhn et al. (2017), which are younger than the Mn nodule formation and which would point towards Mn-nodule burial within the pits.

R2: At sites with stronger bottom currents, e.g. at sites where the near-bottom currents are channelized, nodules do have a higher hydrogenetic content and they are generally smaller and occur in higher numbers (BGR data, e.g. Rühlemann et al., 2012).

AC: What kind of morphological changes would be needed to increase bottom currents, what would be the size of the morphological change? Do we talk about kilometer-, 100m- or meter-scale? This 'scaling issue' makes these results hard to compare with previous studies, which dealt with coarser scales, than this one.

R2: The discussion on the pit structures on page 19, lines 1-13 is wrong. During cruise SO240 one such pit was sampled with box corer and gravity corer. Pore water chemistry was not different from other sampling sites outside the pits (Kuhn et al., 2015). Moreover, heat flow measurements over such pit structures did not show any temperature anomalies. [...]

AC: As mentioned above, we believe the reviewer did not sample a structure in a comparable size in the mentioned cruise. Moreover, it is hard to precisely sample exactly within the pits of such size, especially if the high resolution bathymetry is not available.

Small-scale bathymetry and nodule coverage

R2: Figure 4b indicates that there is a steeper slope in sub-area A2 whereas this area is characterized by higher nodule coverage compared to sub-area A1 (Fig. 5B). This is contradictory to the statement given at page 8, line 26-27.

AC: The trouble is that that ship- and AUV-obtained bathymetry show different correlations. Therefore, it is not possible to apply one statement to different scales. This is one of the main findings of this study and is discussed in section 4.2.4. p.19.

R2: The interpretation of the distribution of the nodule coverage presented in Fig. 7 is based on these weak correlations. How does the predicted low coverage from Fig. 7 correspond with the coverage data from the AUV photo survey? Please provide a scatter plot with nodule coverage from image analyses (x-axis) and nodule coverage from the combination of hydro-acoustic data (y-axis).

AC: This links to the Machine Learning approach, which was not done in this study.

Sediment plume settling

R2: Page 13, line 30: How was the threshold of 8% nodule coverage as complete blanketing defined? Why not 0%?

AC: 8% was the minimum value, because the algorithm sometimes misinterprets shadows as nodules (no area with 0% nodule coverage).

R2: Discussion about particles size in a sediment cloud (page 20/21): The assumption of Stoke's law to describe the sinking behavior of the plume particles is incorrect. Flocculation occurs at large-scale as experimental and modelling results from the JPIO project "Mining Impacts" have shown (pers. comm. A. Vink).

AC: This is written in the text (p.20, line 30/31). Flocculation could also lead to increased friction lowering the sinking velocities, as discussed in p. 20, line 31

R2: Thus, the particles sizes should be much larger than 29 µm on average and the sinking velocities should be rather between 0.5 and 3 m/s. These higher sinking velocities may require a plume height greater than 1.6 m…?

AC: 29 µm is the median particle size in the area, disregarding flocculation (p.20, line 26-27). This scenario and the simple application of Stokes Law was just used to highlight the difficulty in estimating the distribution of a mining-induced sediment cloud, since several factors, such as flocculation / aggregation have to be taken into account and it is hard to make a statement on how such massive sediment plumes will behave in a real mining scenario and what difference these factors make. Nevertheless, the calculated plume height created by the EBS in the experiment is approximately 0.96 to 1.6m (p.20, line 30) in agreement with measured ADCP data (p.20, lines 32-35).

Regarding "sinking velocities should be rather between 0.5 and 3 m/s": How did the reviewer get these values?

Mn nodule growth (page 18-19)

R2: The work of von Stackelberg & Beiersdorf (1991) describes the influence of different parameters on the Mn nodule growth. This work should be taken into account by the authors.

AC: The mentioned work has been taken into account and was cited (p. 17, line 20).

R2: The citation of Mewes et al. (2014) on page 18/19 may not be correct. Mewes et al. (2014) describe that at sites with medium to large-sized nodules a smaller percentage of clay particles have been found in the surface sediments. This may be due to increased activity of near-bottom currents which has removed part of the clay particles. The remaining sediment may have contained a relatively higher proportion of mobilizable Mn which was then available for Mn nodule formation.

AC: "[…]higher sedimentation rate in a low current regime would also mean a higher accumulation of clay size particles, which are proposed to hinder nodule growth Mewes et al. (2014)." To our understanding this means the same in reversion? However, "hinder" has been changed to "not favorable for" (p.29, line1).

3. Technical Corrections

R2: Mixing of abundance and coverage throughout the manuscript. Please correct – see above.
AC: Has been corrected.

R2: Always use the term "ferromanganese nodules" in the text starting with a small letter except at the beginning of sentences.
AC: Mn-nodule was introduced as an abbreviation for ferromanganese nodule in p.2 line 5. It was changed from a capital letter to starting with a small letter, as suggested.

R2: Pay attention to the correct statement of references, e.g., always use parenthesis within a sentence (cf. page 2, line 7 and at many other lines in the text).
AC: Has been changed.

R2: Page 1, line 18: mining operations (no -).
AC: Has been corrected.

R2: Page 2, line 21: 12 km²
AC: Has been corrected.

R2: Page 6, line 8/30: data citation is missing
AC: Has been added.

R2: Page 14, line 7: it must read East instead of West
AC: It is correct as it is. Three different things are named here.

R2: Page 15, line 3: it must read west-facing slope
AC: No, the purple shadings indicate east-facing slopes.

R2: Page 21, line 36-39: Something is wrong with the grammar
AC: These lines are not present? Do you mean another page?

R2: Table A1: AUV MB (Fig. 4, not Fig. 2)
AC: Has been corrected.

R2: Table A2: What is the difference between mineable ridges and ridges, flat depression and depression, mineable deep depression and deep depression?
Table A3: How are the different classes (mineable versus un-mineable) defined?
AC: Thank you for the remark. The following explanation was added to the Figure captions:
DC: p.6, line 3 and p.9, line3: The terms "minable" and "unminable" are defined by slope threshold ("minable": slope <= 3°; "unminable": slope >3°).

R2: Table A6: Why is BPI440st used in this table and not BPI50st?
AC: BPI440st seemed more reasonable for an overview description of the AUV-mapped area, which is why it was used for Fig. 4. BPI50st was used for the small-scale analysis because this BPI-scale detects the single pit structures. Table A6 summarizes the statistics for the descriptive derivatives of the AUV-mapped area, displayed in Figure 4.

R2: Page 29, 1st reference: year is missing.
AC: Reference year is not missing in our document?

Cited References

Kuhn, T., Rathke, M. (2017). Report on visual data acquisition in the field and interpretation for SMnN. Deliverable D1.31 of the EU-Project *Blue Mining*. www.bluemining.eu/downloads. BGR Hannover, 34 pp.

Peukert, Anne. 2016. "Correlation of ship- and AUV-based multibeam and side scan sonar analyses with visual AUV- and ROV-based data: Studies for Mn-nodule density quantification and

mining-related environmental impact assessments." unpublished MSc. Thesis MSc. Thesis, Institute of Geosciences, Christian-Albrechts-Universität zu Kiel.

Reviewer 3

Reviewer 3: Section 1.1 Pg. 2, lines 17-24. As authors mentioned, detailed small-scale investigations are rare in previous work. However, advantages of the small-scale investigation are not described well in the manuscript. It will be helpful if authors can provide some specific issues on nodule distribution which cannot be understood in previous conventional ship-based studies in the Introduction.

Authors Comment: As shown in this study, there are local scale changes in Mn-nodule occurrence, and this variability can be correlated to detailed morphological changes, which is relevant information to understand Mn-nodule forming – processes (p.2, line 18-19).

The local variability studied here is of importance for habitat-studies (section 4.1 p.16, line 5ff) as next to the topographic setting, the nodule availability is of importance for determining local marine habitats i.e. hard grounds. Following your suggestion this has been added in section 1 (p.2, line 18, see DC).

Document Changes: Moreover, the substrate changes considered in this study provide relevant information for estimating size and heterogeneity of local-scale habitats.

AC: Last but not least, only data in the detailed scale considered here can provide reliable information on morphology, which is essential for planning possible mining tracks, since not the entire terrain is suitable and obstacles need to be taken into account for the development of mining gear. This information was added in section 5 p.34, lines 27-29 (see DC).

DC: Areas that appeared suitable of mining (slopes <=3°) in ship-based bathymetric data showed steeper relief (slopes >3°) in higher resolution AUV-based data.

R3: Pg. 2 line 8 the reference should be corrected
AC: Has been corrected.

R3: Pg. 2 line 21 use superscript for km2
AC: Has been corrected.

R3: Section 1.3. Pg. 5. Fig. 2. Geographic Information (i.e. latitude and longitude) needs to be added in the figures showing study area. It will be more helpful if the authors can provide an index map which shows location of study area with some useful information (regional topography or sediment type, for example).
AC: Since the study area is located within the German claim area for resource exploration the exact location is not published within this study (this was discussed with the BGR as contractor of the area). We added the coordinates of the center of the working area in Figure 2 caption (DC). The regional topography is shown in Figures 2 and 3 and is described in the text (section 1.3).
DC: Black squares mark the study area (center 117°1 W 11°51N) shown in Figure 3.

R3: Pg. 6 line 7 and line 30 add the references for data sources
AC: Has been added.

R3: Section 3.1 Nodule coverage:
[…] Thus, I recommend the authors only use the term "nodule coverage", provide a definition or meaning of variation of nodule coverage in this study, and reorganize the manuscript accordingly.

AC: In section 2 p.8, line 31 the Mn nodule coverage considered here is defined (percent coverage per image). Following your suggestion "per image" was added for clarification. We mistakenly used the term "abundance" and changed it to the correct term "coverage" throughout the manuscript.
DC: p.8, line 31: **"**percent coverage per image"

R3: Pg. 8 line 26-27, Fig. 5. The description in the sentence is not clearly shown in Fig. 5C. When variation of nodule coverage is shown together with the bathymetric profile in Figure 5C, it will be easy to see the correlation. Please add color indexing layer above the bathymetric profile in Fig. 5C.
AC: We considered your suggestion and edited Figure 5. The bathymetric profile with the resolution of the AUV-based bathymetry, color coded with the Mn-nodule coverage, was added to the ship-based bathymetric profile.

R3: Pg. 13 line 12 and 14. Please check the figure number.
AC: Has been corrected.
DC: Figure 6B

R3: Pg. 16 Fig. 10. Providing large photos of same location before and after the EBS will be helpful. This can be added in Fig. 10 or be presented as appendix figure.
AC: Considering the navigational error coming along with the AUV data (discussed in p.9, line1), it is not possible to show one photo of the exact same location before and after the EBS experiment even though the exact track was programmed for the AUV survey (p.6, lines 29-30). However, it is reasonable to compare the entire track, where specific patterns (containing of various continuous images) can be used for the recognition of the same areas (p.9, lines 2-3). Due to the absence of large features on the seafloor in the studied area (large enough to not being buried by the resettling sediments) making a recognition of the exact same area possible, such a comparison figure is not shown in this study. We believe the mosaic in Figure 10 shows the burial effect of the EBS-induced sediment cloud sufficiently.

R3: Pg. 16 line 5. I cannot understand the meaning of size of area, 0.49 km2. Does it an area of photo survey in Abyss 168 or Abyss 169 in Fig. 9? If so, please add information.
AC: it means the total area that was covered with AUV imagery. For clarification this information was added as suggested to the mentioned passage.
DC: "0.49km^2 that is completely photo-mapped"

R3: Pg. 17 line 6. What is the CoMoNoD? Need explanation or information for readers who are not aware of the algorithm by Schoening (2017).
AC: It is briefly described in section 2 p.6 line 32ff. For further information the reference is cited and the content of the paper does not need to be given here.

R3: Pg. 17 line 30 check the misspelling "and"
AC: Has been corrected.

R3: Pg. 19 line 13 Water currents can be replaced by Bottom currents
AC: Has been replaced as suggested.

R3: Pg. 19. Some of paragraphs are too long and need splitting. This is especially for the last section of discussion (4.3 Sediment plume re-settling), but also for some other part of the manuscript.
AC: Sub-sections have been added in section 4.3.

R3: Please use parenthesis for reference citation within a sentence.

AC: Has been corrected.

R3: Please use parenthesis for reference citation within a sentence.

AC: Has been corrected.

Understanding Mn-nodule distribution and ~~evaluation of~~ related deep-sea mining impacts using AUV-based hydroacoustic ~~sensing~~ and optical ~~observations~~data

Anne Peukert[1], Timm Schoening[1], Evangelos Alevizos[1], Kevin Köser[1], Tom Kwasnitschka[1], and Jens Greinert[1]

[1]GEOMAR Helmholtz-Center for Ocean Research Kiel, Wischhofstr. 1-3, 24148 Kiel, Germany

Correspondence to: Jens Greinert (jgreinert@geomar.de)

Abstract. In this study ship- and AUV-based multibeam data from the German Mn-nodule license area in the Clarion-Clipperton Zone (CCZ; eastern Pacific) are linked to ground truth data from optical imaging. Photographs obtained by an AUV enable semi-quantitative assessments of nodule coverage at a spatial resolution in the range of meters. Together with high resolution AUV bathymetry this revealed a correlation of small-scale terrain variations (<5m horizontally, <1m vertically) with nodule ~~abundance~~coverage. In the presented data set, increased nodule coverage could be correlated with slopes >1.8° and concave terrain. On a more regional scale, factors such as the geological setting (existence of horst and graben structures, sediment thickness, outcropping basement) and influence of bottom currents seem to play an essential role for the spatial variation of nodule ~~abundance~~ coverage and the related hard substrate habitat.

AUV imagery was also successfully employed to map the distribution of re-settled sediment following a disturbance and sediment cloud generation during a sampling deployment of an Epibenthic Sledge. Data from before and after the 'disturbance' allows a direct assessment of the impact. Automated image processing analyzed the nodule coverage at the seafloor, revealing nodule blanketing by resettling of suspended sediment within 16 hours after the disturbance. The visually detectable impact was spatially limited to a maximum of 100m distance from the disturbance track, downstream of the bottom water current. A correlation with high resolution AUV bathymetry reveals that the blanketing pattern varies in extent by tens of meters, strictly following the bathymetry, even in areas of only slightly undulating seafloor (<1m vertical change).

These results highlight the importance of detailed terrain knowledge when engaging in resource assessment studies for nodule abundance estimates and defining ~~minable~~ mineable areas. At the same time, it shows the importance of high resolution mapping for detailed benthic habitat studies that show a heterogeneity at scales of 10m to 100m. Terrain knowledge is also needed to determine the scale of the impact by seafloor sediment blanketing during ~~mining operations~~mining operations.

1

1 Introduction

1.1 Nodule abundance estimation in relation to benthic structures

The deep ocean is an area of ~~economical~~ economic interest due to ~~the expected amounts~~ its potential reserve of metal resources. Before deep sea mining can be conducted, a better understanding is required of the ecological role of the deep sea as the largest

5 habitat on earth. One focus lies on impacts of ~~Ferromanganese~~ ferromanganese nodule (Mn-nodule) mining which recently has been studied in international projects like MIDAS (http://www.eu-midas.net/) and ~~EcoMining~~ Mining Impact (https://jpio-miningimpact.geomar.de/). Mn-nodules form a hard substrate for sessile fauna ~~Purser et al. (2016); Vanreusel et al. (2016)~~ (Purser et al., 20 their removal is ~~impacting~~ expected to impact respective fauna, but mobile fauna is impacted as well ~~(Bluhm et al. , old).~~ (Bluhm et al., 1995). Quantifying Mn-nodule ~~abundance~~ occurrence and understanding distribution patterns on the seafloor is

10 thus required for ~~ecological assessments,~~ environmental baseline studies as well as ecological and impact assessments.

Several studies correlate bathymetry and nodule ~~abundance~~occurrence, revealing a complex/non-coherent interrelation which mainly depends on the considered spatial scale. Most studies have focused on nodule ~~abundance~~ occurrence variability between very different terrain settings such as seamounts, valleys, plains and undulating terrain ~~Halbach (1988); Pattan and Kodagali (1988); Skorny~~ The detected Mn-nodule variability has been associated with sediment deposition properties, e.g. assuming increased accumu-

15 lation of sediment in flat or depression areas compared to sloping seafloor ~~Frazer and Fisk (1981); Widmann et al. (2014)~~(Frazer and Fisk, 1 Local sediment accumulation influences the dominant formation type of the Mn-nodules (diagenetic vs. hydrogenetic), their size and metal concentration ~~Jung et al. (2001); Kim et al. (2012); Mewes et al. (2014); Widmann et al. (2014). Detailed~~ (Jung et al., 2001; but detailed small-scale investigations (1m to 100m scale) are not commonly done. ~~Okazaki et al. (2013)~~ (Okazaki et al., 2013) propose to perform such investigations to improve our knowledge about Mn-nodule formation processes and the affecting parameters.

20 ~~The study presented here jointly~~ Moreover, the substrate changes considered in this study provide relevant information for estimating size and heterogeneity of local-scale habitats.

The study analyzes ship-based bathymetric data for large scale background information together with AUV-obtained high resolution multibeam (MB) and optical data to reveal detailed nodule coverage patterns within a ~~12km2~~ 12km^2 area. The resolution of the acoustical AUV data enables the identification of vertical morphological undulations of less than 1m with a

25 lateral resolution of 3-5m. Results from optical and hydroacoustic data were analyzed to assess correlations between Mn-nodule ~~abundance~~ coverage and small-scale morphology and to extrapolate Mn-nodule occurrences to a wider area.

An equivalent approach was applied for an environmental impact study on sediment blanketing during a simulated 'mining-operation'. Mn-nodule mining will affect the seafloor and benthic fauna in several ways. A removal of the upper-most sediment layer (5-20cm) will cause habitat loss for sessile fauna which depends on nodules as hard substrate (Figure 1; ~~Vanreusel et al. (2016)~~(Vanreu

30 and for organisms living in the uppermost 'fluffy' sediment layer. The suspended sediment plume can clog filter organs of suspension feeders and the re-depositioning of suspended sediment will bury sessile organisms. These physical impacts could further be accompanied by bio-geochemical disequilibria in the water column and the sediment surface that will impact the local environment on short and long time scales ~~Shirayama and Fukushima (1997); Kotlinski et al. (1998); Sharma et al. (2001); Thiel and Tiefse~~ The release of toxic substances or metals might also ~~be of importance~~add to the impact. Together these effects can increase mor-
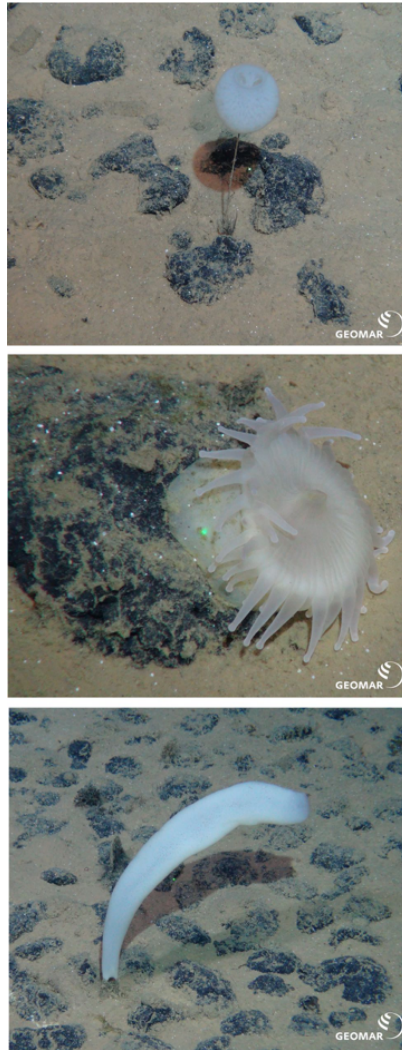
2

Figure 1. Sessile benthic organisms depending on manganese nodules as a hard substrate habitat. Images from the German claim area in the Clarion Clipperton Zone (photos: ROV Kiel 6000, GEOMAR-Helmholtz Center for Ocean Research Kiel, Germany)

tality with unknown short term and cumulative effects ~~Markussen (1994); Sharma (2011)~~(Markussen, 1994; Sharma, 2011). Increased water turbidity ~~and the short-lived yet massive~~ in the water column and the re-deposition of ~~sediment that needs to be large volumes of re-suspended sediment in a relatively short time interval is~~ expected during mining and are uncommon in the deep sea. Estimating the ~~size~~ extent and distribution pattern of ~~such a~~ the re-settled ~~sediment plume~~ particles of such sediment plumes is therefore relevant for assessing deep-sea mining impacts on a larger spatial scale.

1.2 Previous Benthic Impact Experiments and environmental studies

Various Benthic Impact Experiments (BIEs) have been ~~set up~~ conducted to study sediment re-suspension and the distribution of sediment plumes in Mn-nodule areas (e.g. ~~Ozturgut et al. (1980); Foell et al. (1990); Fukushima et al. (1995); Sharma (2001))~~ ~~. To determine the plume distribution and blanketing pattern,~~ (Ozturgut et al., 1980; Foell et al., 1990; Fukushima et al., 1995; Sharma, 200 for which data were acquired by ~~scattered mooring stations~~ (few) moorings equipped with different sensors, sediment sampling

5   as well as by optical observations using video and photo material. These data finally contributed to the development of sediment plume distribution models ~~Lavelle et al. (1981); Jankowski et al. (1996)~~ (Lavelle et al., 1981; Jankowski et al., 1996) and led to interpolated blanketing maps ~~Barnett and Suzuki (1997); Yamazaki et al. (1997)~~(Barnett and Suzuki, 1997; Yamazaki et al., 1997). Observations from these ~~large-scale~~ larger-scale (as compared to thos study) BIEs (OMI, OMA, OMCO (1978), DISCOL (1989), BIE-II (1993), JET (1994), IOM-BIE (1995), INDEX (1997), MMAJ (1997)) indicated different distribution distances

10   of the created bottom plume ranging from several tens ~~of meters Barnett and Suzuki (1997); Trueblood et al. (1997); Sharma (2001)~~ or hundreds of meters (Barnett and Suzuki, 1997; Trueblood et al., 1997; Sharma, 2001) up to several kilometers away from the disturbances ~~Burns (1980); Lavelle et al. (1981); Jankowski et al. (1996); Yamazaki et al. (1999).~~ (Burns, 1980; Lavelle et al., 1981; Janko

The use of different disturbance gear for different duration per BIE leads to inconsistent interpretations ~~Jones et al. (2000)~~(Jones et al., 20

15   Unfortunately, definitions for 'a sediment plume' differ with regards to minimum particle size and amount of particles ~~. Thus~~and thus, parameters are applied differently in model approaches. While some models calculate the distribution of the re-suspended material until all sediment particles have settled from the water column (pers. comm. A. Dale, SAMS), others define certain particle concentration thresholds (Burns 1980). A concise plume definition could be based on thresholds (e.g. with regard to amount of particles, shape and size distribution) that benthic organisms could tolerate on short but also longer cumulative time

20   scales. Defining such thresholds requires in-situ experimental data of the reaction of benthic fauna to sediment plumes in the area of potential mining. Detailed studies do not exist but are essential for estimating the ecological consequences of deep sea mining.

Plume model results are based on several assumptions to include parameters describing the environment. Particle sizes and settling velocities are key factors in modelling plume distribution distances ~~Jankowski et al. (1996)~~ (Jankowski et al., 1996) and

25   uncertainties can lead to miss-interpretations. Our current understanding of the behavior of re-suspended particles in the deep sea is based on laboratory experiments. Often, these experiments struggle to correctly determine settling velocities of flocculating particles, and/or they rely on specific deep sea sediments and might not account for the correct environmental parameters. Nevertheless, modeling the distribution of a plume induced by Mn-nodule mining is the only way to predict the possibly impacted area. Meaningful models need to incorporate all environmental aspects and need to operate at the highest possible

30   resolution.

The study presented here focuses on an area within which the resettled sediment was visually observable in deep sea photographs of the seafloor. Two AUV photo surveys over the same area were conducted before and after the deployment of an Epibenthic Sledge (EBS), that created a sediment plume. The two data sets are directly compared to determine the scale of the

visible disturbance. The correlation of the photo data with AUV-obtained bathymetry data reveals the influence of the local terrain variability on the sediment blanketing pattern and thus the sediment plume spreading.

1.3 Study area description

The study area is part of the Prospective Area 1 (~~PA 1~~PA1) within the German license area in the eastern Clarion Clipperton Zone (CCZ). The wider area (Figure 2) has a mean water depth of 4240m with abundant isolated or chains of seamounts of vari-

5 ous heights. Mostly N-S-trending parallel graben and horst structures originating from the East Pacific Rise (~~Rühlemann et al. (2011)~~(Rühle Figure 2) can be seen as well. The ~~PA 1itself~~PA1 itself is a plateau-like area, elevated approximately 150m above the surrounding terrain and classified as a 'mineable plateau' in Figure 2D. ~~At a small scale~~Small scale undulations (<100m) ~~the morphology of the plateau is~~ on the plateau are smooth with slopes of <10° in wide parts of the area. ~~Increased~~A stronger relief is associated with seamounts or ridge structures (Figure 2). To the West, the plateau is bounded by a deep graben structure,

10 whereas towards the East and the South the terrain ~~drops~~slopes down to depressions with irregularly scattered seamounts of different sizes (red areas in Figure 2D).

High resolution studies using data from several AUV deployments were carried out within the '~~minable~~mineable plateau' (black square in Figure 2). This plateau is characterized by slopes of less than 3° and the area is considered suitable for Mn-nodule collector systems ~~Kuhn et al. (2011)~~(Kuhn et al., 2011). The AUV study area is located west of a ridge that follows the

15 characteristic N-S lineation and is only little structured showing a smoothly undulating terrain (Figure 3). Towards the North the AUV study area is bounded by a slightly ~~higher area; itself~~elevated area, which dips towards the South, leading into a wider depression. Smaller basins/depressions are found throughout the entire area. Slopes are generally <10° and those exceeding this value are found only in association with a group of seamounts in the South-West (Figure 3). The zoomed-in view in Figure 3 is based on newly acquired EM122 data ~~(; DATA CITATION)~~ (Greinert, 2016) showing a terrain more variable as initially

20 assumed from the data set shown in Figure 2 (data from an EM120, 2° by 2° beam angle system). The more variable data ~~already points~~also point towards a further terrain differentiation and potentially a less homogenous Mn-nodule ~~abundance~~ coverage within the area. The acquired AUV multibeam data that were processed to a horizontal resolution of 5m provide the small-scale morphology. The resulting bathymetric maps were used for correlating nodule coverage and sediment blanketing patterns of the disturbance experiment.

2 Methodology and Disturbance Experiment

All ship- and AUV-based surveys were conducted in March 2015 during the 'EcoResponse' cruise SO239 with R/V SONNE ~~Martínez Arbizu and Haeckel (2015)~~(Martínez Arbizu and Haeckel, 2015). Large-scale bathymetric data were acquired by the hull-mounted Kongsberg EM 122 Multibeam Echosound (MBES) system (12kHz, 0.5° along- and 1° across-track beam angle; 55m cell size). The swath angle was set to 120° and the survey speed was about 8kn. A REMUS 6000 type AUV was

30 deployed for the high resolution mapping and photo surveys (http://www.geomar.de/en/centre/central-facilities/tlz/auv-abyss/). A RESON Seabat 7125 MBES system was used (200kHz, 2° along track and 1° across track beam angle). The AUV-based
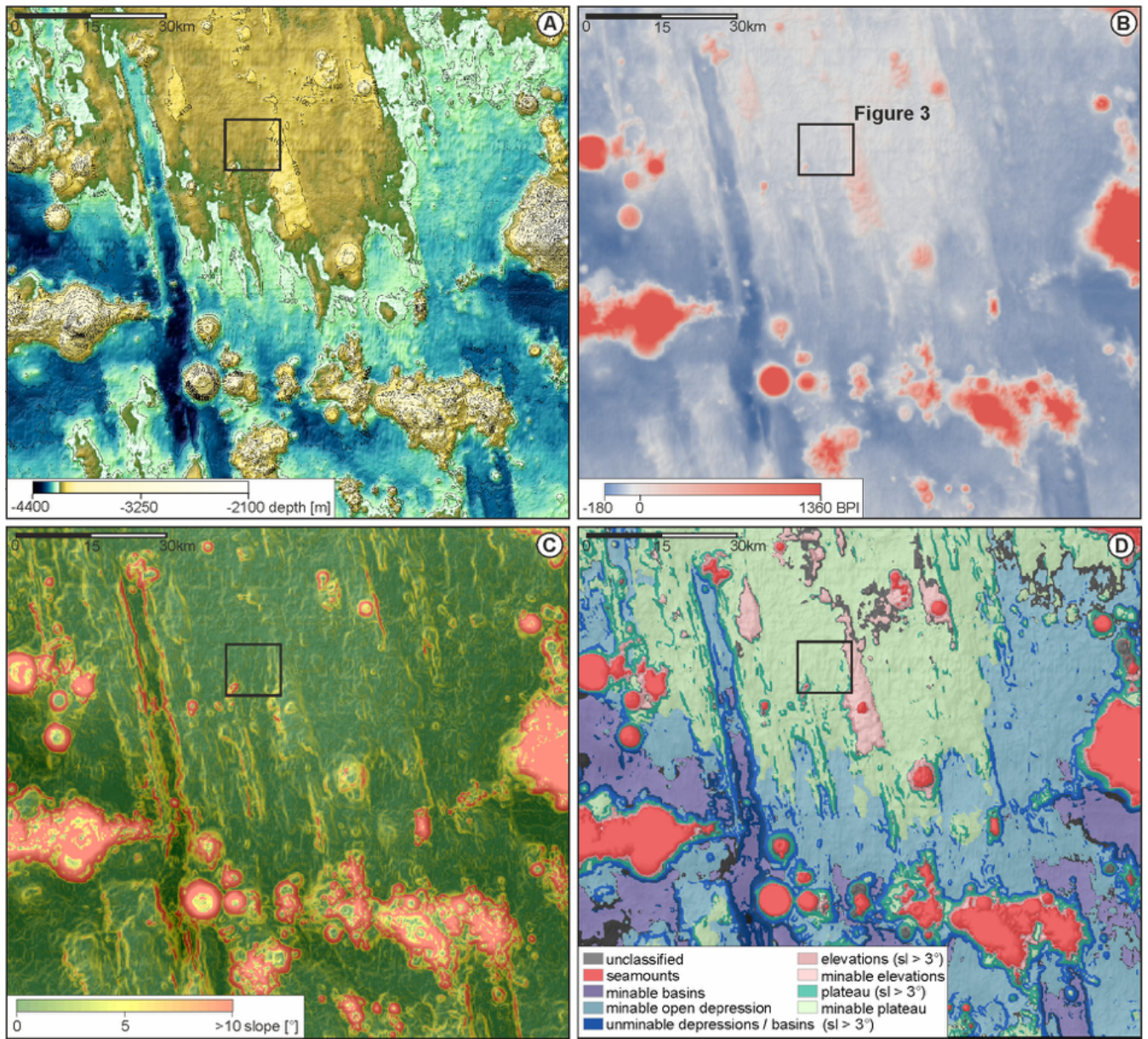
Figure 2. Overview maps of PA 1 showing A: Bathymetry, B: Bottom Positioning Index (BPI) with ~~scalefactor~~ scale factor 11,000 (grid cell size: 110m, inner radius: 10 cells, outer radius: 100 cells), C: Slope and D: Classification of the terrain based on the classification dictionary in Appendix Table A2 (sl = slope). The terms *mineable* and *unmineable* are defined by the slope threshold (here *mineable* = slope $\leq 3°$; *unmineable* = slope $> 3°$; this is rather conservative threshold, current discussions mention $7°$ as more realistic). Black squares mark the study area (center 117°1W 11°51N) shown in Figure 3.
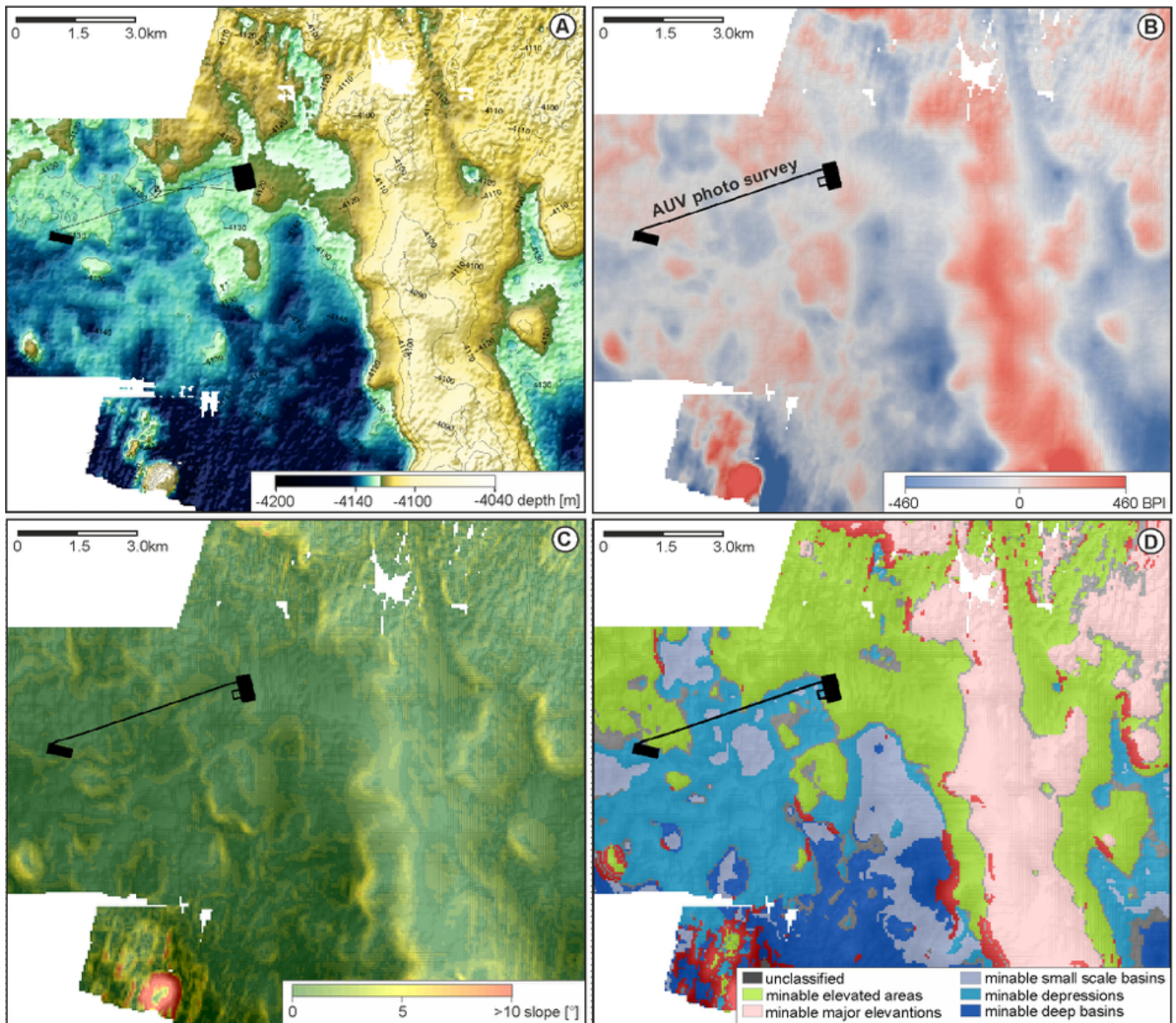
Figure 3. Overview maps for the geological setting of the AUV study area. A: Bathymetry; B: Bottom Positioning Index (BPI) with ~~scalefactor~~ scale factor 2,750 (cell size: 55m, inner radius: 10 cells, outer radius: 50 cells); C: Slope (in degree); D: Terrain classification based on the classification dictionary in Appendix Table A3. Black lines indicate the track of AUV Dive 168 prior the EBS ~~deplyoment~~ deployment (A) and the locations of usable photos from this dive (B, C and D). See Figure 2 caption for the definition of "mineable" area.

multibeam surveys were conducted at an altitude of 80m above the seafloor. Bathymetric maps were produced with the software packages GMT 5.2 ~~Wessel et al. (2013)~~ (Wessel et al., 2013) and ArcGIS 10.2. The MBES data were analyzed in ArcGIS 10.2 as a floating point raster (see Appendix for cell size of different regions, Table A1). Data were projected as UTM coordinate

system (Zone 11N) to enable spatial analysis. Bathymetric first order derivatives (slope, aspect) and second order derivatives (Bathymetric Position Index - BPI, Vector Ruggedness Measure - VRM, total curvature, plan curvature, profile curvature) were calculated for each region and sub-region using tools in SAGA GIS and ArcGIS (spatial analyst toolbox and the 'Benthic Terrain Modeler' Add-on toolbox ~~Wright et al. (2012)~~(Wright et al., 2012); for further details see Appendix and Table A4).

The AUV camera system 'DeepSurveyCam' ~~Kwasnitschka et al. (2016)~~ (Kwasnitschka et al., 2016) was used for visual
5   seafloor inspection by two photo surveys. Photos were taken from 7 to 9m altitude at a mean speed of 3kn, gaining more than 50,000 usable photos. Two sub-areas A1 and A2, located approximately 5km apart, were photographed extensively. One part of both AUV-surveys in sub-area A2 followed exactly the same track before and approximately 16h after the deployment of an Epibenthic sledge ~~(DATA CITATION AUV IMAGERY and Mn-Counting)~~(Greinert et al., 2017; Schoening, 2017a, b). Photos were automatically analyzed for the Mn-nodule coverage on the seafloor (percent coverage) and nodule size distri-
10   bution (different quantiles in ~~cm2~~cm^2, see Appendix for details). The 'Compact Morphology Nodule Delineation' algorithm was used for this task ~~Schoening et al. (2017)~~(Schoening et al., 2017). This nodule delineation method is based on color differences between the nodules and the sediment background. Derived quantitative values are georeferenced and can thus be jointly analyzed with the AUV-obtained bathymetry. This allows understanding correlations between nodule abundance and the decameter-scale morphological changes in the AUV studied area.

15   As a side product of benthic sampling using a B-EBS Type sledge ~~Brenke (2005)~~ (Brenke, 2005) a sediment plume was created. The sledge itself has a length of 360cm and a width of 120cm with a weight of approximately 420kg in water. It creates a pressure of about 13g/~~cm2~~ cm^2 onto the sediment surface (see Appendix Figure A3). The sledge was towed during station SO239_024-EBS across sub-area A2 (Figure 4A) from West to East at ca. 0.5m/s leaving a track of approximately 20cm in depth ~~Martínez Arbizu and Haeckel (2015)~~(Martínez Arbizu and Haeckel, 2015). The re-settlement of the sediment plume
20   was visually mapped using the camera system and automated image analysis mentioned above.

3   Results

3.1   AUV-based bathymetry and overview of Mn-nodule ~~abundance~~coverage

The water depth within the AUV-mapped area ranges from 4110m to 4143m (Figure 4A) with 93% of the area showing slopes <3° (Figure 4B). Steeper slopes between 7° and 10° occur locally in the East and towards the North as well as in randomly
25   distributed pit structures, which occur throughout the area (Figure 4). These pit structures take up approximately 10% of the area and attain sizes from several tens of meters to 150m in diameter with a maximum depth of 4m. They occur exclusively within larger depressions (ca. 50% of the area) as visualized by the BPI map (Figure 4C).

The two AUV photo surveys provide visual data from within the high resolution MBES map (black lines, Figure 4A) covering a depth range from 4134m to 4114m. The first AUV camera survey (SO239_019_Abyss168) provided data over two extensive sub-areas in the West (A1) and East (A2), as well as one survey line connecting both areas (Figures 4A & 5). The second survey remapped parts of sub-area A2 (SO239_028_Abyss169) and additionally mapped a similarly sized area further south ~~Martínez Arbizu and Haeckel (2015)~~(Martínez Arbizu and Haeckel, 2015). Based on the automated image analyses the
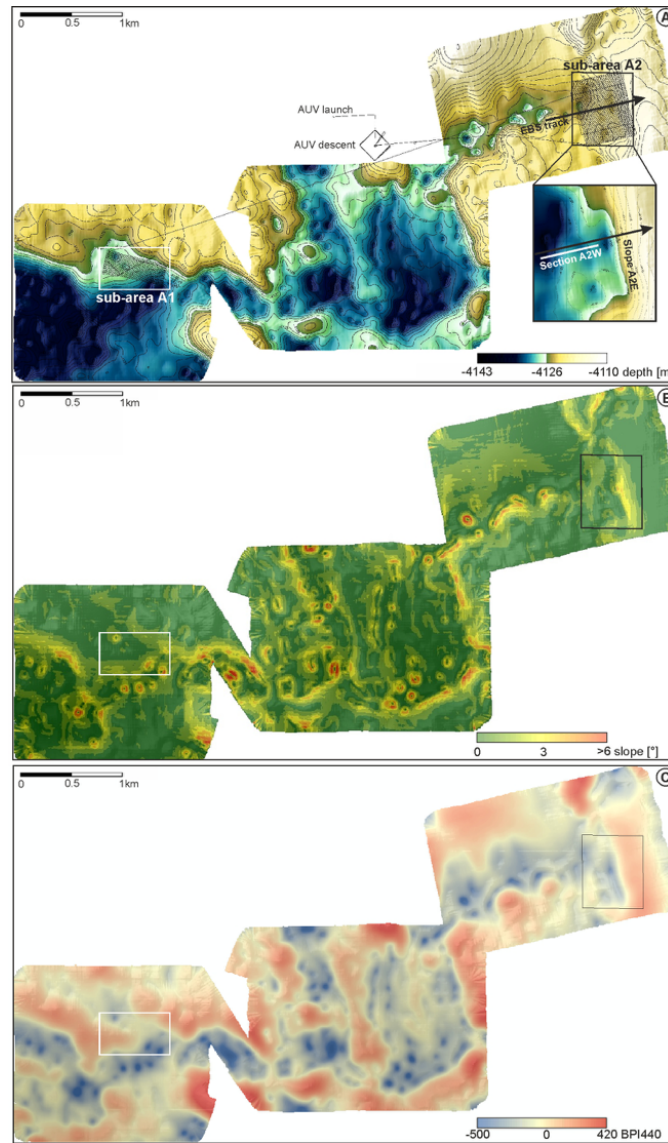
Figure 4. Bathymetric map obtained by the AUV with black line indicating the track of AUV Abyss Dive 168 prior to the EBS ~~deplyoment~~deployment. The black arrow marks the tow track of the EBS deployment. B): Slope map derived from bathymetry indicating maximum slopes of $10°$; C): BPI map (BPI440) derived from AUV-obtained bathymetry. The black and white rectangles indicate the Eastern and Western sub-areas.

5   majority of the seafloor shows nodule coverage values between 8% and ~~16~~17% (Figure 5A)~~with a greater proportion of higher coverage values (13 to 16%) in the eastern A2 sub-area~~. Values below and above this range (<1%) have been neglected, since they are caused by "unusual" objects (like EBS-tracks or organisms) in the images.
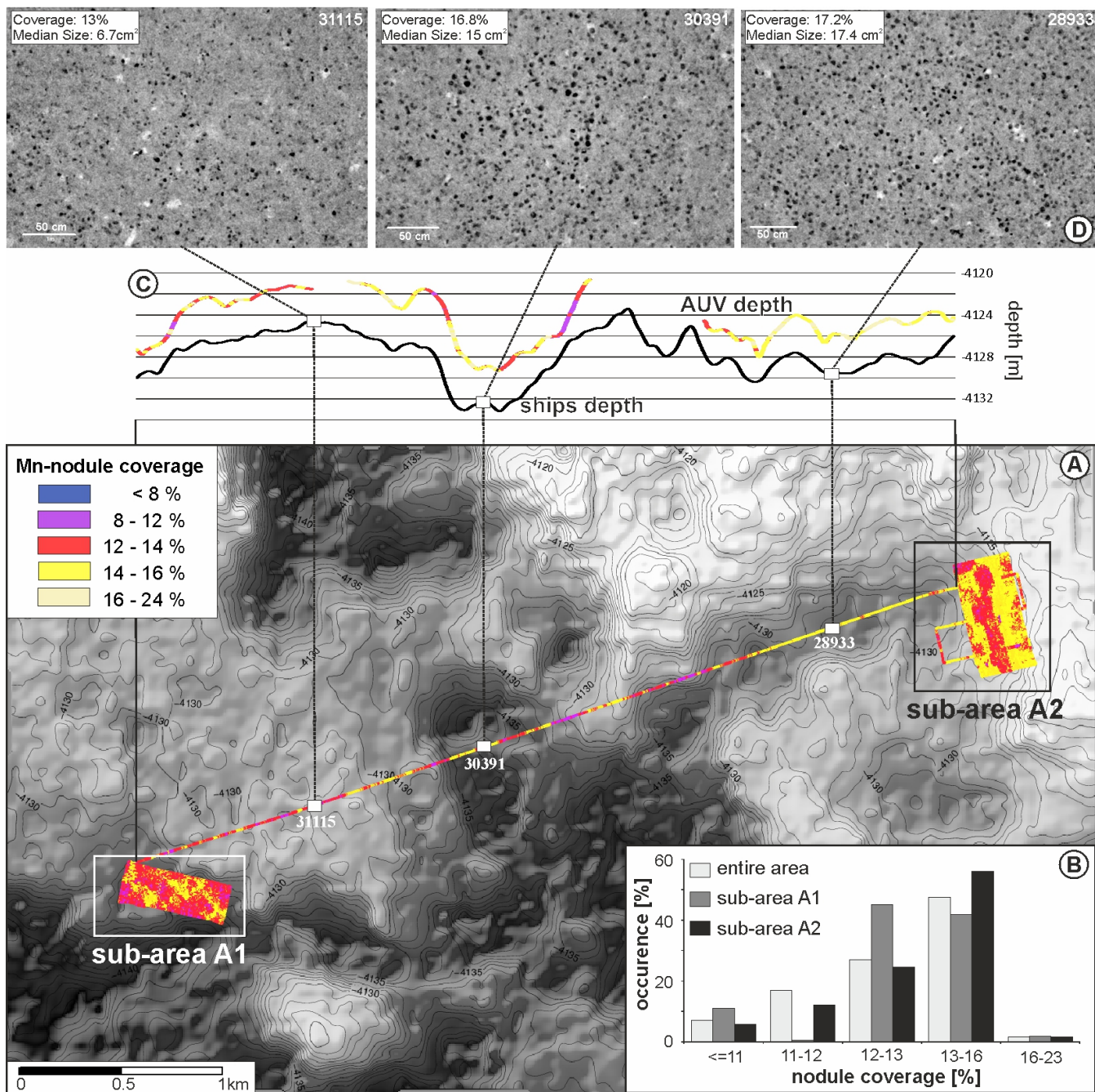
9

Figure 5. A) Bathymetric map (ship-based MBES) of the Working Area with nodule coverage calculated from AUV photo survey; the photo examples in D) show the Mn-nodule coverage and median size in different areas. B) Statistical evaluation of nodule coverage for the entire photo survey (green bars; 30,038 photos) and the sub-areas A1 (gray bars; 10,120 photos) and A2 (red bars; 16,890 photos).
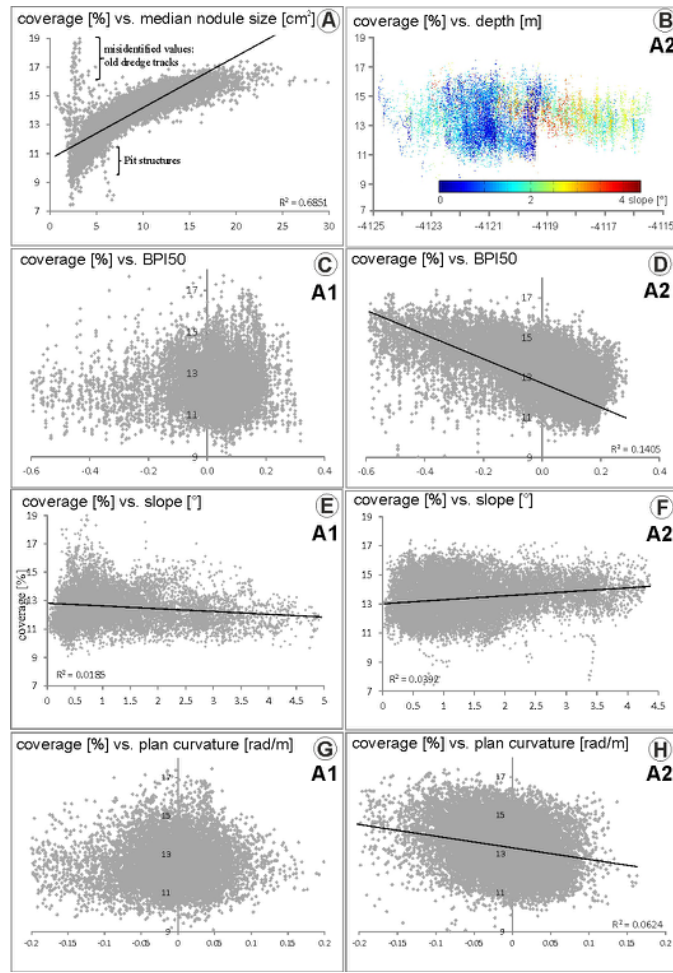
Figure 6. Scatter Plots indicating relationships between Mn-nodule percent coverage (%) and eight other nodule and terrain values: median nodule size in ~~cm2~~ cm² (A), depth within the A2 sub-area (B, color-coded by slope), BPI50 (C,D), slope (E,F) and plan curvature (G,H). Charts (C,E,G) relate to sub-area A1; charts (B,D,F,H) to sub-area A2. The sub-areas show different correlations.

In the following examinations the threshold between 'low' and 'high' Mn-nodule coverage is set at 12.5%~~;~~ which is the analyzed mean coverage value ~~.~~ of the considered range. In the eastern A2 sub-area a greater proportion of higher coverage values (13-16%) can be observed. A positive correlation was found between Mn-nodule coverage and median size of the nodules (Figure 6A). The correlation decreases with increasing nodule size, indicating a compensation of the size by a decreasing number of occurrences. This is consistent with findings of former studies e.g. by ~~Okazaki et al. (2013)~~(Okazaki et al., 2013).

3.1.1 ~~Large~~ Broad scale variability (less detailed, correlation with ship-based bathymetric data, resolution 100-1000m)

Parts of dive SO239_019_AUV2 run across the entire working area providing data from different terrains that can be linked to the ship-based bathymetric information. The correlation between photo analysis and this less resolving bathymetry indicates a trend of decreasing nodule coverage at elevations and steeper sloping areas (Figure 5). Video-data acquired during previous cruises provide similar observations ~~Kuhn (2015)~~(Kuhn, 2015). The distribution pattern seen in the imagery also points towards small scale Mn-nodule coverage variability which is possibly related to minor topographic changes in meter to sub-meter scale. As only one track covers the central region of the working area clear correlations between Mn-nodule occurrence and large scale ship-based bathymetry are difficult to assess. Finding clear correlations is further complicated by the uncertainty of the AUV navigation (up to 30m), which prevents a precise geo-referencing of the photos between sub-area A1 and A2. More robust visual reference data could be provided by conducting a sparse mesh survey across the entire area or by a contiguous photo mosaic across different terrains.

3.1.2 ~~Small~~ Local scale variability (more detailed, correlation with AUV-based bathymetric data, resolution 1-100m)

The assessment of small scale Mn-nodule coverage heterogeneity was based on the western A1 and eastern A2 sub-areas; here, overlapping photo-mosaics and AUV-based bathymetric data in meter resolution exist (Figure 4A). Sub-area A2 (700m x 500m, 0.35~~km2~~km^2) is bound to the East by a 5-7m high 'ridge' with a relatively steep slope ('Slope A2E', 3°-7°). The western part of this area ('A2W') shows only minor morphological variation and a total relief of ca. 2m (Figure 4). Despite the rather small relief changes, variations in Mn-nodule coverage can be observed (Figures 5 & 7).

Figure 7A illustrates the detailed bathymetry of the studied area with red dots indicating lower Mn-nodule coverage ($\leq 12.5\%$) as indicted by image inspection. Those areas with a BPI50 > 0, slopes $\leq 1.8°$ and plan curvature values > -0.02 radians/m were found to show the best correlation with the lower Mn-nodule coverage in sub-area A2 (Figure 6D, F, H). A NW-SE oriented, elongated patch in the central part of A2 that corresponds to a flat-topped (slope $\leq 1.5°$), slightly convex shaped elevated structure (<1m above the surrounding terrain) shows a low Mn-nodule coverage. A higher Mn-nodule coverage instead occurs at steeper slopes (>1.5°) and in morphological depressions (negative BPI values, negative plan and total curvature) indicating a sediment depositional environment. Two distinct depression structures (Pit 1 and Pit 2 structures in Figure 7), both approximately 60-80m in diameter and 1-2m deep, show a different pattern; here, the visible Mn-nodule coverage is significantly lower (0-8%). The almost spherical pit structures are bound by slopes of >2° and thus produce slightly increased Vector Ruggedness Measurement values >1x10-4 (VRM; Figure A4 A) and the lowest observed BPI-values (Figures 4C & A3 B). Similar structures are observed throughout the entire study area (blue shaded areas in Figure 7 and circular features seen in the slope map of Figure 4B). Based on additional ROV and benthic camera surveys it is assumed that these pit structures exhibit very few to no Mn-nodules ~~(Peukert, 2016).~~Peukert (2016).

No further correlation between Mn-nodule coverage and bathymetric derivatives was found ~~; no relation exists~~ and no relation to absolute water depth ~~(Figure 7~~could be observed (Figure 6B). However, Figure ~~7~~6B shows a significantly lower
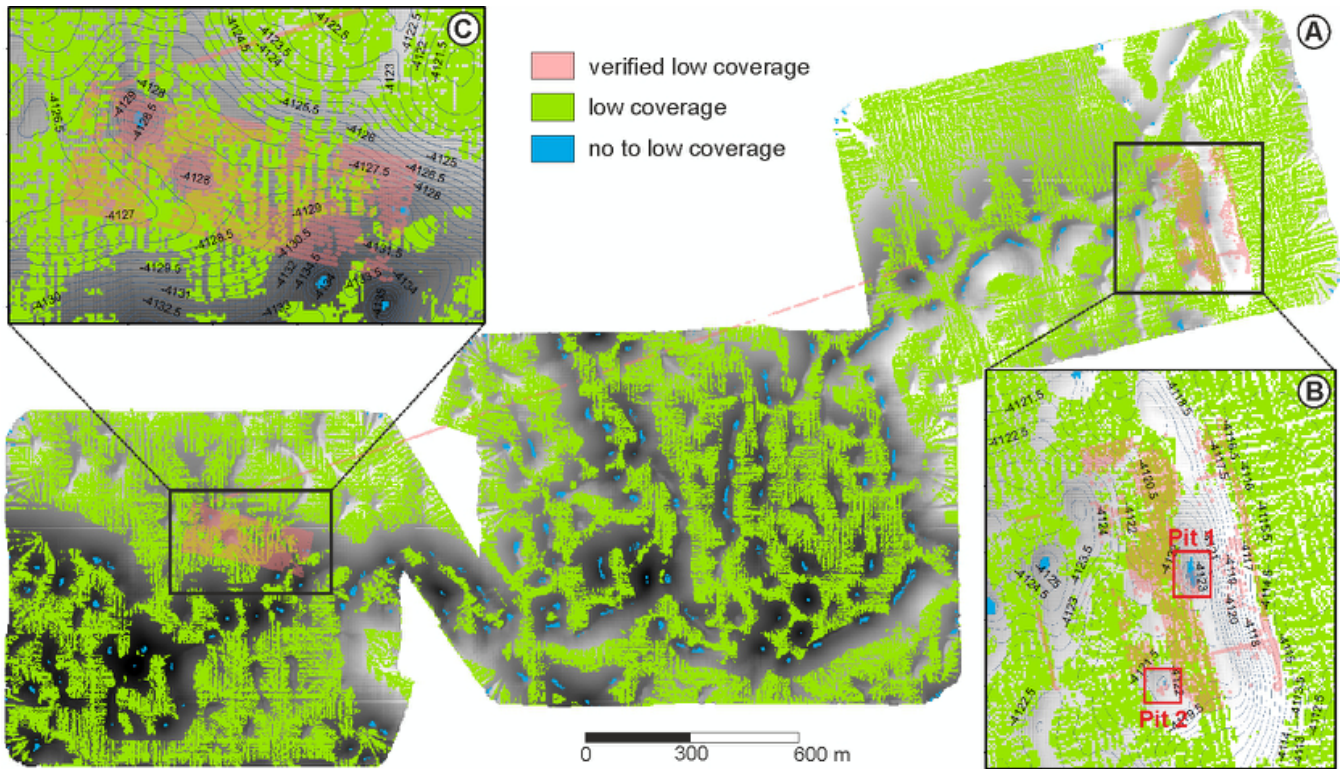
Figure 7. (A): Depth-shaded area, mapped hydro-acoustically by the AUV; (B): A2 sub-area, (C): A1 sub-area. The green shading indicates low nodule coverage areas (<=12.5%) that have been classified based on the correspondence in sub-area A2 (low nodule coverage corresponds with slopes <= 1.8° and positive plan curvature). Red boxes in B mark distinct, almost nodule-free, morphological depressions (Pit 1 & 2). Blue shades indicate areas with a high probability of very low to no Mn-nodule coverage. See classification dictionary in Table A5.

variability of Mn-nodule coverage for water ~~depth above~~ depths shallower than 4019m (only ca. 4% variability, compared to 6-7% variability in deeper areas); these areas correspond to steeper slopes (ca. 2° to 3.5°) associated with the eastern bounding
30   elevation ('Slope A2E', Figure 4A) of sub-area A2. Along this west-facing slope the Mn-nodule coverage clearly increases with increasing depth. Areas featuring low slope values show higher variability in Mn-nodule coverage ~~.~~(Figure 6B).

A lower Mn-nodule coverage (<12.5%) is predicted for the green areas marked in Figure 7A when using the BPI50, slope and plan curvature classification of the A2 sub-area (Figure 7B). Although the resulting area does not match completely with the areas of low coverage derived from the photo analyses (red dots/shades in Figure 7), it represents the best correlation that
35   could be achieved. Based on this result, a Mn-nodule coverage of <12.5% can be expected in 39% of the study area (green shades in Figure 7) and is likely to be very low or zero in at least 1% of the area (blue shaded parts).

In sub-area A1 (230 x 600m, 0.138~~km2~~km^2) no correlation is observed between the photo analyzed ~~Mn-coverage~~ Mn-nodule coverage (red) and the seafloor classification of A2 (green; Figure 7C). In addition, scatterplots (Figure 6C-H) show different dependencies between Mn-nodule coverage to BPI, slope and plan curvature between A1 and A2. In both areas though, the

13

5 coverage attains more uniform values towards steeper slopes (Figure 7 E, F). A stronger correlation is shown in A2, and an inverse correlation in A1. In both areas the highest variability but also the lowest values of Mn-nodule coverage occur in generally flat areas (curvature values around 0, low slope values; Figure 7E, G).

Comparing the terrain statistics of areas A1 and A2 (Figure 8) reveals differences in their bathymetric settings, which might cause this discrepancy. Sub-area A2 mainly slopes towards West to Southwest, as indicated by the aspect distribution and to a
10 lesser degree in 'opposite' Northeast to East directions caused by the general pattern of N-S striking graben and horst structures. In comparison, the main slope direction in A1 is towards ~~southerly directions~~a southerly direction. The slope distribution in A1 indicates a dominance of slopes up to one degree. This is reflected by the large area of flat seafloor as determined by the AUV-BPI440 value distribution (Figure 8). In A2 slopes are steeper, the terrain is more variable and a larger number of depressions are observed compared to A1. The VRM shows similar values for both areas (Table A6). These differences in bathymetric derivative values point at a lower terrain variability in A1, confirmed by the more consistent depth values in A1 relative to A2. Considering the generally lower Mn-nodule coverage within A1 (Figure 5A) it is concluded that lower Mn-nodule coverage
5 correlates with lower terrain variability and lower slope values. This generalized observation is consistent with findings for A2. Although a direct one-to-one relationship valid in both sub-areas could not be derived, the general trend indicates higher Mn-nodule coverage with more variable terrain, along smooth slopes and in concave shaped terrain (depressions).

3.2 Sediment plume re-settling

To evaluate sediment plume re-settling, results of the automated image-based Mn-nodule detection before the EBS disturbance
10 (SO239_019_Abyss168 with 6,061 usable photos) and after the EBS disturbance (SO239_028_Abyss169 with 10,783 usable photos) were compared (Figure 9A). Areas with the lowest analyzed coverage were associated with sediment blanketing that covers the Mn-nodules completely (here defined as <8% Mn-nodule coverage, green shaded areas in Figure 9).

The AUV-tracks of the photo surveys run perpendicular to the EBS track. A strong sediment blanketing can be observed close to the disturbance track (Figures 9 & 10). The photo mosaic shows a sharp transition between low (no) and higher Mn-
15 nodule coverage north of the EBS track ~~in a distance between~~ over a distance of 5m to 20m (Figure 10). South of the track the transition from complete sediment blanketing to areas without visible sediment cover is gradually fading out with increasing distance to the EBS-track; a slight sediment blanketing of Mn-nodules can be observed up to 70m away from the EBS track (Figures 9 & 10). This pattern indicates a southward directed bottom current, which is confirmed by ADCP-based current measurements (station SO239_005; see Appendix Figure A5). An upward looking 300kHz ADCP (15min ensembles, 2m bin
20 sizes) was positioned 500m SE of the EBS track at the time of the EBS deployment ~~Martínez Arbizu and Haeckel (2015).~~ (Martínez Arbizu and Haeckel, 2015).

The combination of AUV-obtained bathymetry and imagery reveals a distinct blanketing pattern depending on the small scale morphology (Figure 9). In section A2W, where the total relief is only 1-2m, the re-suspended material was distributed 20m to 30m towards the north of the EBS track and 40m to 50m towards the south of it. West of A2W, within Pit 1 and the
25 adjacent slope area A2E (Figure 9, red shaded area) the seafloor slope increases to max. 6° and the water depth decreases by several meters (Figure 9). This morphological change causes the sediment plume to cover the seafloor only up to 6m towards
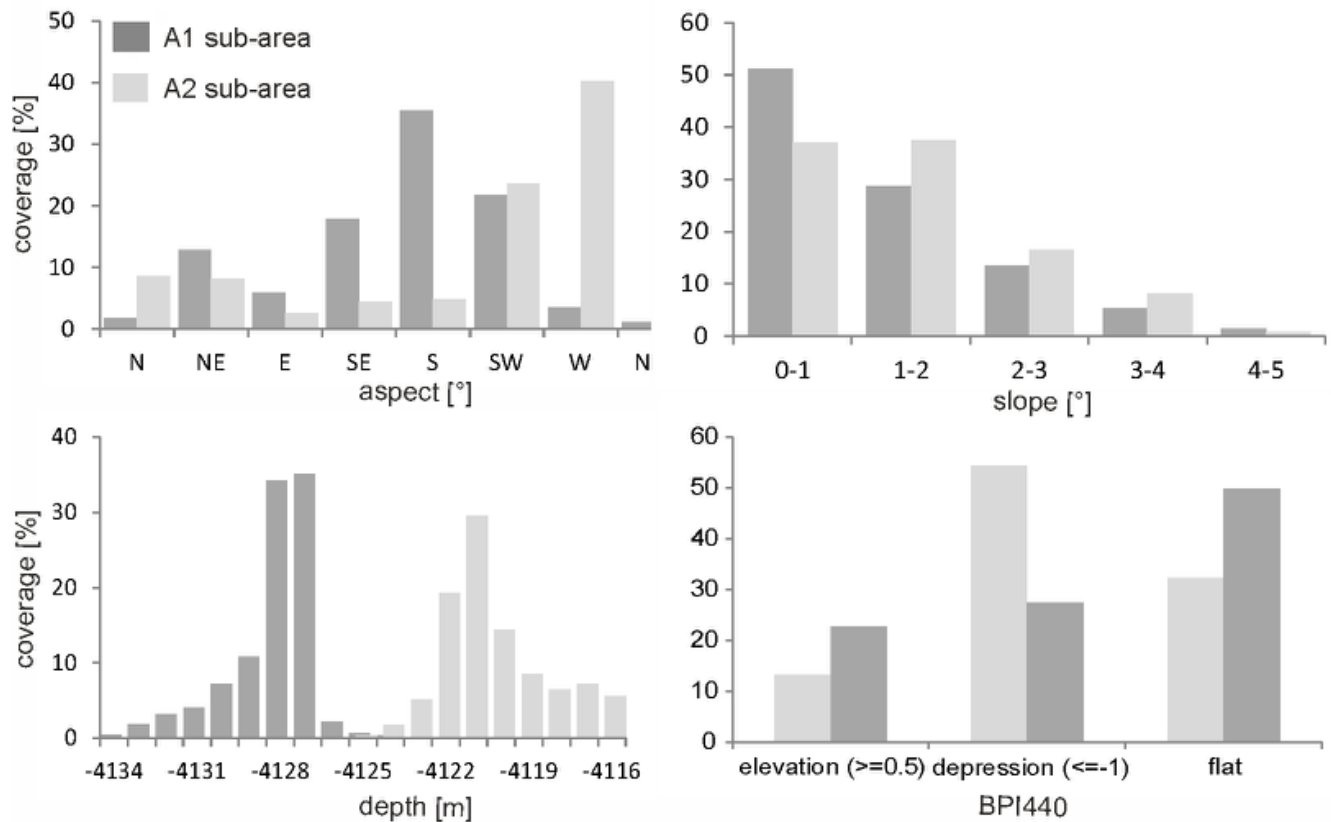
Figure 8. Distribution of derivative values in sub-area A1 and A2.

the north of the EBS track. The greatest distance at which sediment has been deposited away from the EBS track occurs within Pit 1 (Figure 9). Here the least visible Mn-nodule coverage extends up to 70m south of the EBS track, significantly further than in the flat section A2W and slope area A2E.

4   Discussion

4.1   Uncertainties of photograph-based Mn-nodule coverage and size estimates

Seafloor photographs have been used for Mn-nodule ~~abundance~~ occurrence studies for almost two decades ~~Park et al. (1997); Sharma et al. (~~ The presented AUV imagery reveals the natural Mn-nodule heterogeneity at the seafloor surface on a very fine scale (decimeters) over an extensive area (of 0.49~~km2)~~km^2 that is completely photo-mapped. This highly detailed insight is of importance for a spatially detailed evaluation of the small scale habitat distribution and potentially allows a better resource assessment. However, potential uncertainties for the absolute numbers of Mn-nodule size and coverage are explained here.
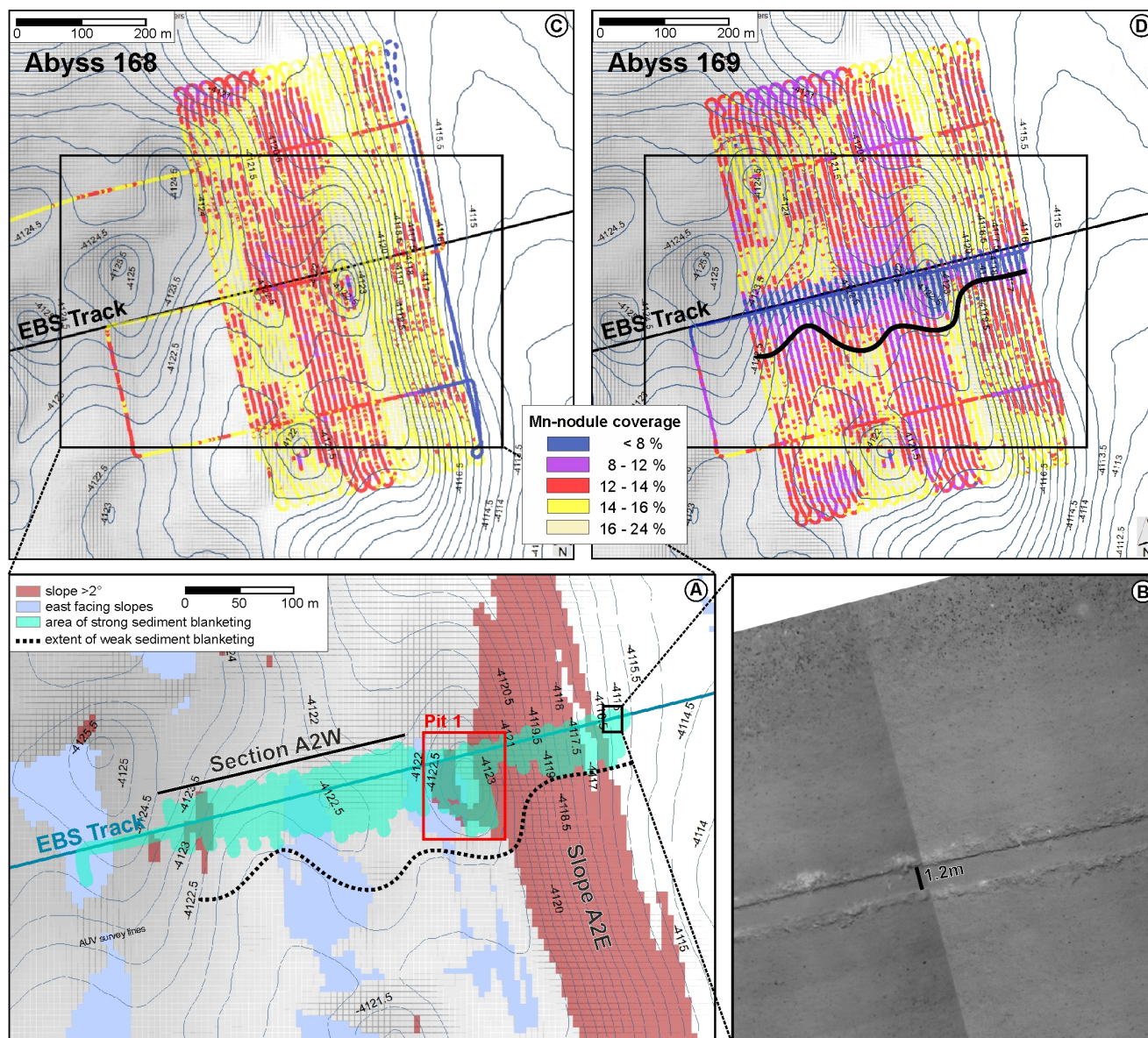
15

Figure 9. (A) The green shaded area in the detailed bathymetric map marks lowest nodule coverage sites, associated with the sediment cloud dispersal. The dashed black line represents the furthest extent of weak nodule blanketing. It corresponds to a nodule pixel color brightening and can be automatically computed from the imagery. Purple shading indicates east- facing slopes. Red shade marks areas with slope >2°. The blue line marks the ideal track of the EBS deployment. (B): Extract from a photo mosaic created from AUV imagery; nodules are completely covered by sediment towards the sides of the tracks; approximately 10m north of the track the sediment cover disappears within a sharp transition. Maps in (C) and (D) show the analysed Mn-nodule ~~abundance~~ coverage before (C; dive SO239_019_AUV2) and after (D; dive SO239_028_AUV3) the EBS deployment.
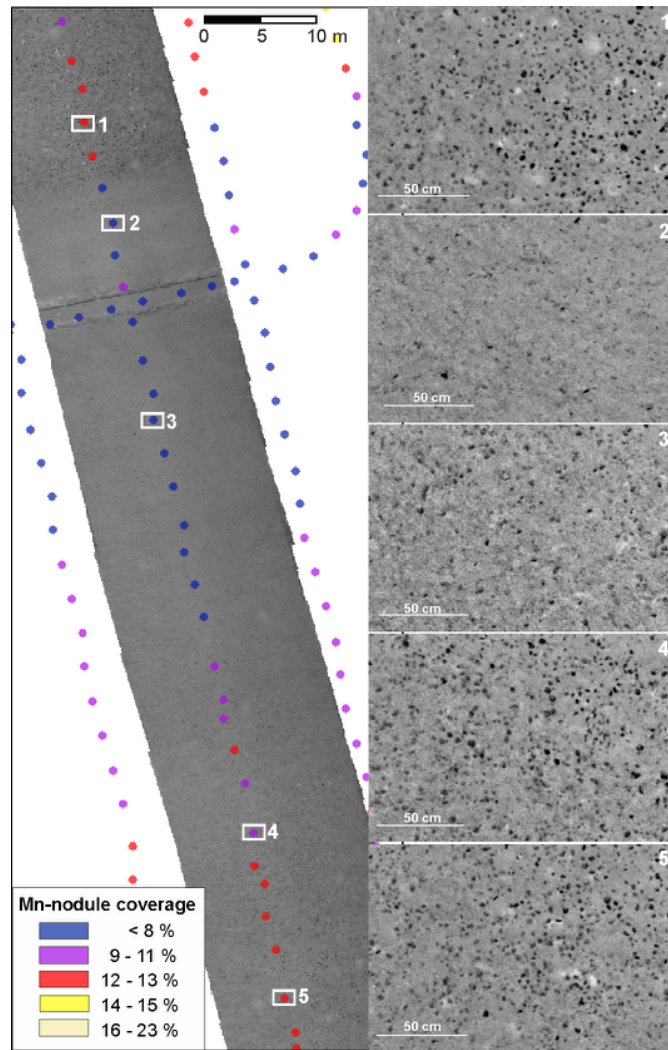
Figure 10. Section of the photo mosaic along one survey track line, with calculated nodule coverage values, indicated by the color coded dots (representative for the center of each individual photo which are ca. 15m x 11.5m (~~172m2~~172m^2) in size). White squares mark positions of the enlarged photos shown to the right.

Photographs only provide information of the sediment surface and thus will not be able to detect buried/sediment-covered Mn-nodules ~~Sharma and Kodagali (1993); Sharma et al. (2010, 2013) for more~~ (Sharma and Kodagali, 1993; Sharma et al., 2010, 2013), resulting in a potential underestimation of the absolute Mn-nodule abundance (Kuhn and Rathke, 2017). For absolutely accurate resource assessments and verification of the presented results, detailed sampling based on this study would need to follow. With respect to mapping Mn-nodules as hard grounds for sessile fauna, photographs give a realistic quantitative representa-
5 tion of size/coverage and spatial nodule abundance changes. Nevertheless, the automated image analysis CoMoNoD has some uncertainties ~~Schoening et al. (2017)~~(Schoening et al., 2017). In general, the nodule identification employed here is based on

contrast differences between the nodules (dark) and the sediment (bright). Mn-nodules on the seafloor could be located too close to each other to be correctly separated by the applied algorithm and, depending on the image quality and the contrast thresholds, quantitative coverage and size distribution values can be inaccurate ~~Sharma et al. (2010); Schoening et al. (2012); Tsune et al. (2014); Scho~~

10   A6). Turbidity in the water, backscatter from particles, the water properties and the altitude of the camera (AUV) impact image quality ~~(Edwards et al. (2003); Kwasnitschka et al. (2016)~~(Edwards et al., 2003; Kwasnitschka et al., 2016). Nevertheless, optical imaging provides information on relative changes in seafloor Mn-nodule coverage and nodule sizes. This makes the presented technique an effective monitoring tool for habitat and environmental impact assessments that investigate the re-settling of suspended sediment. We detected a distinct trend of higher coverages correlating with larger nodules (Figure 7A) that could

15   be a result of imperfect segmentation if the nodule density is too high.

4.2 Correlation between bathymetry and nodule occurrence

4.2.1 ~~Broad~~ Regional scale correlation between ship-based bathymetry and Mn-nodule coverage/size

In general, properties such as sedimentation rate ~~Frazer and Fisk (1981); Mewes et al. (2014)~~(Frazer and Fisk, 1981; Mewes et al., 2014), type and thickness of the sediment ~~Frazer and Fisk (1981); Jeong et al. (1994)~~ (Frazer and Fisk, 1981; Jeong et al., 1994) are

20   believed to determine Mn-nodule growth ~~von Stackelberg and Beiersdorf (1991)~~(von Stackelberg and Beiersdorf, 1991); for sediment deposition environments the interplay between bottom currents and bathymetry plays an important role ~~Halbach (1988)~~(Halbach, ... The depositional properties vary on a regional scale, considering large geomorphological terrain types, but are also impacted on a local scale of only a few kilometers and even less ~~Craig (1979); Frazer and Fisk (1981); Sharma and Kodagali (1993); Mewes et al. (2014~~ Varying considerations of scale and regional differences in nodule exposure between different oceans across different studies

25   have thus led to partly contradicting statements of the relationship between the Mn-nodule coverage/size and bathymetric settings.

Several investigations report small Mn-nodules and low coverages in depressions and plains which are considered as sediment accumulation sites, in contrast to seamounts, slopes and crests ~~Pattan and Kodagali (1988); Sharma and Kodagali (1993)~~(Pattan and K... Other studies discussed comparatively larger diagenetic Mn-nodules in plains which are also considered as sediment accumula-

30   tion areas. More abundant but smaller hydrogenetic Mn-nodules have been observed in more rugged terrain ~~Skornyakova and Murdmaa (199~~ Such terrains are interpreted to increase current velocities andd turbulences caused by channel effects reducing sediment accumulation. ~~Mewes et al. (2014)~~

(Mewes et al., 2014) present a correlation between Mn-nodule size and sedimentation rate, where large nodules correlate with a smaller amount of clay fraction in the sediments that they interpreted to be caused by stronger bottom currents/lower sedimentation rate. A similar observation is presented by ~~Skornyakova and Murdmaa (1992)~~ (Skornyakova and Murdmaa, 1992) who state that diagenetic/large Mn-nodule formation is linked to a periodical redistribution of the surface sediment layer.

5   With respect to the large scale of the ship-based bathymetry in Figure 2, the working area of this study is located in a sediment-accumulating flat terrain with smooth bathymetry, characterized by the occurrence of medium to large (>4cm) Mn-nodules ~~Rühlemann et al. (2011)~~(Rühlemann et al., 2011). However, a more detailed view allows the identification of terrain

variability on a scale of several tens to hundred meters that enables a more detailed assessment of the associated Mn-nodule coverage variability (Figure 5). Larger nodules/higher coverage values occur in depressions and at sloping seafloor when compared to broad scale bathymetry. Larger nodule sizes could be the result of stronger bottom currents preventing/reducing the deposition of sediment on nodules and/or favoring nodule growth. For another area in the German claim, box core (BC) samples taken by the Federal Institute of Geosciences and Natural Resources (BGR Hannover, Germany), revealed larger (diagenetic) nodules in a very broad scale flat terrain. This area has been classified by ~~Widmann et al. (2014)~~ (Widmann et al., 2014) as an area of sediment accumulation and is compared to a rougher, supposedly sediment 'winnowing' area, with many smaller nodules formed hydrogenetically. The interpretation of sediment accumulating and winnowing areas is based on broad scale ship-based bathymetry of much coarser resolution compared to this study.

According to the study by ~~Skornyakova and Murdmaa (1992)~~ (Skornyakova and Murdmaa, 1992) the data presented here indicate lower sedimentation rates associated with stronger bottom currents in the depressions supporting the growth of larger Mn-nodules. Increased bottom currents within the depressions could possibly be induced by convergent channeling or turbulences of bottom currents, which contradicts the assumption of lower current strength and therefore higher sedimentation within depressions.

4.2.2 ~~Fine~~ Local scale correlation between AUV-based bathymetry and Mn-nodule coverage/size

Variability in Mn-nodule ~~abundance~~ coverage within several tens of meters or less can be correlated with AUV-based bathymetry. In sub-area A2, patches of low Mn-nodule coverage correlate with low bathymetric elevations even when the relief differs by less than one meter. The strongest correlation between low Mn-nodule coverage was determined with slightly convex shaped elevated structures (surfaces <1° slope, positive plan curvature and positive BPI values). These parameters most likely define ~~small-scale~~ local-scale sedimentation environment affecting the local balance between sediment accumulation and erosion The presented data show that favorable nodule growth/occurrence conditions coincide with gentle sloping sites and low relief depressions, where sediment is assumed to accumulate slowly.

Within sub-area A2 a smaller variability of Mn-nodule coverage can be observed in correlation with the 'Slope A2E' towards the East. This is in agreement with observations by ~~Sharma and Kodagali (1993)~~ (Sharma and Kodagali, 1993) who also observed more uniform nodule ~~abundances~~ coverages in sloping areas. The authors point out that this could be a result of a larger exposure of the Mn-nodules rather than absolute difference, since they discovered discrepancies between direct sampling and results of photo analyses.

Rather special for the presented data set are the pronounced pit structures, observed throughout the AUV-mapped area with very little to no Mn-nodules observed at the sediment surface. This is in contradiction to the wider depressions, where a higher Mn-nodule coverage was observed. The existence of such pronounced depressions most likely leads to a reduction of bottom current velocities resulting in a higher sediment deposition of suspended sediment and potentially even sediment slumping from the sides. This could result in sedimentation rates too high for Mn-nodule formation ~~Halbach (1988); Mewes et al. (2014)~~ (Halbach, 1988; M a simple cover/burial of previously formed and still existing Mn-nodules ~~at depth.~~ below the sediment surface. The formation process of the pits is unclear, but could be karst structures (Kuhn et al., 2017), which are younger than the Mn-nodule formation

which would point towards Mn-nodule burial within the pits. At the same time a higher sedimentation rate in a low cur-

10 rent regime would also mean a higher accumulation of clay size particles, which are proposed to ~~hinder nodule growth Mewes et al. (2014)~~not be favorable for nodule growth (Mewes et al., 2014). Another possibility could be that these pit structures are pockmarks, formed by pore water release (~~Harrington (1985); Hovland and Judd (1988)~~ (Harrington, 1985; Hovland and Judd, 19 a significant change in local pore water geochemical properties and eventually warmer temperature that prevented Mn-nodule formation in the past. Unfortunately the pit structures could not be sampled in more detail and it is unknown whether Mn-

15 nodules exist at all or if different geochemical conditions are present within the pits. Similar, but larger structures exist in the DISCOL area ~~Greinert (2015)~~ (Greinert, 2015) showing very similar geochemical conditions as other Mn-covered areas in both highly detailed sediment surface analyses as well as deeper sediment cores.

4.2.3 Comparison between sub-areas A1 and A2

When comparing the relationships between the bathymetric derivatives and the Mn-nodule coverage it becomes evident, that

20 correlations visible in A2 cannot be seen in A1 (Figure 6A, C)~~; here~~, where areas of lower nodule coverage could not be matched with distinct terrain types. This result points towards additional parameters that influence Mn-nodule occurrence. Geochemical processes could be involved that drive the Mn-nodule formation; these in turn depend on the sediment properties (composition, sedimentation rate, porosity, etc.). ~~Water currents~~ Bottom currents could additionally influence the sedimentation rate and affect the geochemical processes in the benthic boundary layer and Mn-nodule surface. Local differences in the

25 hydrodynamic regime near the bottom seem likely, as the bathymetric derivatives vary between the two sub-areas. Sub-area A2 is bound towards East and North by elevated terrain (7m to 10m higher) which could have a focusing effect on bottom currents eventually causing a more erosional environment. In contrast, sub-area A1 is unbound by elevated terrain within 2km distance. This might cause a stronger influence of seasonally changing bottom currents, preventing a clearer correlation of Mn-nodule coverage with the seafloor morphology.

30 4.2.4 Broad- vs. small-scale correlation

The observations made on broad scale (several hundreds of meters; grid cell size of 55m) show that high Mn-nodule coverage correlates with depressions (Figure 5) which is consistent with observations on smaller-scale (scale of tens of meters, grid cell size of 5.5m) for sub-area A2 (Figure 7). Outside of A2 decreasing Mn-nodule coverage correlates with steeper sloping areas, which is contradicting to observations on small-scale, where the lowest Mn-nodule coverages correlate with extremely low slope angles of less than 1.8°. This contradicting finding highlights that simple and generalized correlations between Mn-

5 nodule occurrence and bathymetric but also geochemical properties in the sediment might not be possible on regional scale (10km to 1000km) but on local scale (100m - 10km). This is because the formation parameters also change on such local scales which are not possible to accurately predict using ship-based multibeam data, 'sparse' box-coring (distances of few kilometers) and limited information about current regimes.

4.3 Sediment plume re-settling

10 The approach of conducting a photo mosaic survey before and after a seafloor disturbance proved successful for detecting sediment blanketing visually, offering the possibility to accurately map the area of strongest plume-impact. This area is characterized by the sediment plume transport direction and re-settling of the majority of the sediment. Very fine particles within the sediment plume might be dispersed much further; more detailed biological studies need to evaluate which sediment concentrations and grain sizes will impact benthic organisms on long time scales (cumulative effects) outside the visually clearly 15 detectable impacted areas.

The thickness of the resettled sediments could not be determined from the AUV-based images or ROV-based video footage during the cruises. Video observations from other, similar areas point towards a sediment cover on millimeter or sub-millimeter range that can still be detected in images (e.g. in laboratory experiments ~~Yamazaki et al. (1997)).~~ (Yamazaki et al., 1997)).

4.3.1 Morphology-influence on sediment transport

20 The extent of the visible sediment blanketing, that varies over several tens of meters, can be related to a focusing of the sediment plume settling or the prevention of it through small-scaled morphological changes in form of barriers (steeper slopes facing against the current) or the opening of plume transportation pathways (sloping terrain with the current). Varying terrain in general will modify the current regime near the bottom and thus the settling properties of the sediment plume; it might also enhance the interactions between the particles due to increased turbulences that might stimulate increased flocculation and 25 thus scavenging of very small particles that otherwise would be much further distributed. The shorter transport of sediment in north- and southward direction from the EBS track along the 'Slope A2E' implies that the transportation of the suspension load follows the slope downhill. In 'Sub-section A2W', where the terrain is very smooth (the relief changes by 1m to 2m) a dependency of the sediment blanketing extent to structures of the undulating seafloor could still be observed. At the western end of Sub-section A2W the east-facing slopes act as barrier for an undisturbed migration of the sediment plume with the bottom 30 current towards the South. The spreading of the sediment blanketing is wider in the East of Sub-section A2W where the seafloor is almost horizontal, before slightly dipping towards the East and into the Pit 1 structure. The slopes considered show angles of less than 2° and the morphological variability is sometimes less than 1m. More distinct features, like Pit 1 (Figure 9), cause a more variable sediment plume dispersal. The sediment blanketing within this 2m deep feature does not exceed the southward edge of the depression. The re-suspended sediment seems trapped within this feature with possible additional suspension load coming from the neighboring eastward slope.

4.3.2 Estimation of plume height

In a first approach we estimated the plume height generated by the EBS by considering the extent of the observed sediment 5 blanketing and measured bottom current velocities at the time of the EBS deployment (31mm/s; measured by ADCP). Former models from the CCZ reported settling velocities of particles in a sediment plume in the range of 0.1 to 1mm/s derived from visual and experimental data ~~Lavelle et al. (1981); Oebius et al. (2001)~~(Lavelle et al., 1981; Oebius et al., 2001). Preliminary

results of particle size analysis from a comparable site within the PA 1 indicate a median grain size of 29μm (Benjamin Gillard, Jacobs University Bremen, Germany, personal comm.). Following Stokes' law and disregarding aggregation of the particles,

10   the determined median particle size for the area would translate to sinking velocities of approximately 1mm/s. Assuming an average dispersal width of 30-50m downstream, as indicated for the A2W sub-section (Figure 9), this would require a plume height of approximately 0.96 to 1.6m. Aggregation processes leading to larger particle sizes are likely to occur which, due to increased friction, would sink slower than similar sized 'Stokes' particles but that would scavenge a substantial amount of very small particles (personal comm. Laurenz Thomsen, Jacobs University Bremen, Germany). As part of studies in the south Pacific

15   DISCOL area, lander-based ADCP backscatter measurements detected a passing-by sediment plume induced by a similar EBS experiment as discussed here. These data indicate a plume height between 1.5m to 2m ~~Greinert (2015)~~(Greinert, 2015).

4.3.3   Implications for possible mining scenario

It can be assumed that, due to the higher turbulences caused by the deployment of an industrial collector system and the continuous release of suspended material into the water column during mining, the dynamic behavior of the sediment plume

20   could be altered and adjusted in such a way that the suspended sediment is re-settling in the fastest possible way, keeping the dispersion to a minimum. Determining the dynamic behavior of the plume under different collector-dispersion scenarios by monitoring in-situ and under real-mining conditions is thus essential to improve our understanding and model capacity with regards to the near- and far-field plume distribution and finally to evaluate ecological short- and long-term impacts.

These ecological impacts can be significantly ~~spatially confined~~ confined to a small area by reducing the height of the

25   sediment plume, increasing the settling velocity and aggregation of particles (scavenging the very fine sediment fraction. Vertical discharge of sediment after its separation from the Mn-nodules should be avoided; instead a horizontal discharge close to the bottom (<10m from the bottom; below 'stable' stratification above the well mixed bottom boundary layer) with a velocity as slow as possible (speed of the collector) should be aimed for. One first implementation of this concept was the setup of the DSSRS disturber ~~Brockett and Richards (1994)~~ (Brockett and Richards, 1994) deployed in a few large-scale Benthic Impact

30   Experiments (BIE-II, JET, IOM-BIE, INDEX).

As indicated by our results, a low-height sediment plume will be trapped in small depressions. Thus a detailed knowledge of the local morphology on small scales is a pre-requisite to correctly determine the area and thickness of re-settling sediment. This is also relevant in planning adjacent mining tracks from a miner's point of view, since strong sediment blanketing might burry adjacent nodules to be mined. According to our results, this impact will be highest in sediment accumulation sites, but even on 'flat' areas with slopes of less than 3° the distribution of the sediment plume and the resulting sediment blanketing

5   distance will vary on a range of several tens of meters. In areas with steeper slopes (e.g. 10°), the sediment blanketing distance can be even wider.

In our very small scale experiment, the EBS created a local impact with clearly visible sediment blanketing within 100m downstream off the track. This localized impact is also the result of only partial re-suspension of the surface sediments that was directly caused by the EBS (1.2 in width). Observations of EBS tracks during another experiment revealed that a larger

10   part of the sediment is compressed by the EBS and pushed aside with only a smaller (unknown) fraction being suspended

Boetius (2015)(Boetius, 2015). It can be speculated that re-sedimentation of particles outside the visible blanketing area is minor, will happen over longer time, and thus might not have a significant effect on the benthic organisms and the ecosystem (short and long-term cumulative impacts on specific fauna still needs to be determined).

The actual scenario of disturbance will be different during real-case mining during which the top 10 - 20cm of the sediment are removed, then 'filtered for nodules' and are then discharged at the seafloor. One single track will be about 17m wide as e.g. planned in a German concept Kuhn et al. (2011)(Kuhn et al., 2011), whereas the track width of the EBS was only 1.2m. As not only one track will be mined, but the collector system will operate constantly in 'lawn-mowing' pattern of long tracks scraping off the seafloor surface, the entire mined area will see a strong impact Jankowski and Zielke (2001)(Jankowski and Zielke, 2001). Considering local topography, bottom currents, optimizing particle settling You (2004) (You, 2004) for fast and effective floc-culation by the collector, and the cleaning of the sediment plume from the water column by settling phytodetritus from plankton blooms (increased flocculation) the size of the impacted area and the impact itself caused by the sediment blanketing outside the mined area might be rather small (<10km) and controllable. For a final validation, an experimental setup closer to the expected mining conditions is needed Sharma (2011)(Sharma, 2011); the presented study shows that we have the understanding, tools and the methodologies at hand to perform monitoring studies needed for such a realistic deep sea mining experiment.

5   Conclusions

We conclude that for both of our study topics, the Mn-nodule abundance/distribution to terrain comparison as well as the re-deposition of sediments indicate that Mn-nodule coverage and sediment blanketing vary measurably on very small scale (several tens to hundreds of meters), even if the seafloor terrain changes are minor (less than 1m vertical change). This supports the second conclusion: that spatial scale needs to be considered when discussing possible parameters that influence Mn-nodule abundance coverage as such, and that relations found in one region most likely cannot be generalized to other regions and across different scales. Confirming previous studies, our data also show no simple relationship between Mn-nodule abundance and coverage with the seafloor morphology even when working on the same spatial scale. It needs to be realized that a complex interrelation between morphological characteristics and local environmental conditions (physical, chemical, sedimentological) influence the visually detectable Mn-nodule abundance coverage at the seafloor surface. Reasons for this are that 1) variable amounts of Mn-nodules have formed under different geochemical, bottom current or sedimentological conditions in different places, 2) Mn-nodules might have dissolved in certain areas because of changing geochemical conditions or mechanical ero-sion, 3) Mn-nodules were buried by sediment whereas the sediment deposition pattern is influenced by the seafloor terrain and its interplay with bottom currents and 4) the existence of Mn-nodules (abundance, size, total coverage) itself influences sediment erosion, making denser covered areas with large nodules more resistant against sediment erosion.

With respect to the sediment plume study it became obvious that a visible blanketing occurs in a limited distance (here <100m) away from the disturbance track and that the blanketing pattern strongly depends on bottom current direction, strength, small-scale bathymetry and initial plume height. From these observations it can be concluded that each sediment plume disposal via an exhaust/diffusor of the collector should occur horizontally as close to the bottom as possible, rather than on top of the

vehicle, blowing the sediment particles high into the water column, aiming for a finer dispersal over larger areas. Our studies also highlight that the performed disturbance experiment cannot be scaled up to a real mining scenario and that more detailed studies are required to understand and quantify the cumulative impact of unsettled particles on filter-feeding organisms beyond
15 the clearly visual blanketing area.

On the technical side the study showed that we have the needed tools and techniques at hand to map the seafloor for Mn-nodule resource assessments and a better understanding of Mn-nodule distribution as well as for assessing mining impacts visually. It became clear that without such high resolution techniques valid assessments cannot be carried out. Areas that appeared suitable of mining (slopes ≤3° in ship-based bathymetric data showed steeper relief (slopes >3°) in higher resolution
20 AUV-based data. For an 'environmentally friendly deep sea mining' such high resolving maps are a pre-requisite to accurately define areas that need to be protected, and maneuver mining infrastructure around them considering the actual bottom currents and sediment settling areas during the mining.

Code and data availability. Source code for the automated nodule delineation is available in Pangaea (Schoening, 2017c). The data used in this work is available in Pangaea. This includes MBES data (Greinert, 2016), optical imagery (Greinert et al., 2017) and image-derived
25 nodule coverages (Schoening, 2017a, b).

Appendix A: Methodology

A1   Calculation of the bathymetric derivatives

Slope was calculated using the algorithm included in the 'Spatial Analyst' Toolbox ~~Burrough (1986)~~ (Burrough, 1986) of ArcGIS (Table A4 output in 'degrees'). Curvature as second order derivative of the bathymetry represents the slope of the slope.
30 It has also been determined with the ArcGIS 'Spatial Analyst' Toolbox. For each cell a 4th order polynomial is fit to a surface composed of a 3x3 cell window. From this surface the tool calculates the coefficients (Table A3), which are set into relation with the elevation values for every cell ~~Zevenbergen and Thorne (1987)~~(Zevenbergen and Thorne, 1987). The two maximum slope dependent curvature values of the plan curvature, perpendicular to the maximum slope, and the profile curvature parallel to the maximum slope direction were calculated. The plan curvature defines flow convergence (concave surface, values < 0) and divergence (convex values > 0). Profile curvature affects the acceleration of the flow with values < 0 indicating a concave shaped surface and values > 0 indicating convex shaped surface. In addition the total curvature of a surface has been calculated which is also > 0 when convex shaped or < 0 when concave shaped. Curvature values of 0 are indicative for flat surfaces.
5 For calculating aspect, Bathymetric Position Index (BPI) and Terrain Ruggedness the ArcGIS 'Benthic Terrain Modeler' (BTM) Add-in ~~Wright et al. (2012)~~ (Wright et al., 2012) and its incorporated algorithms were used. The classification performed by the BTM is based on manually set properties (Tables A1 & A2) of the derivatives slope, BPI (fine scale and broad scale) and water depth. This simple classification process provides sufficient information to distinguish different terrain settings of the study area (Figures 2 & 3). The classification of the AUV-mapped study area (Figure 6, Table A5) was per-

10   formed to reveal areas of lower Mn-nodule coverage and is based on the derivatives BPI, slope and plan curvature, since these morphological parameters showed the best correlation with Mn-nodule coverage (Figure 7). For the BPI calculation of the AUV-mapped area the algorithm used within the BTM was modified (without integer rounding) to preserve the small-scaled features ~~Wilson et al. (2007).~~ (Wilson et al., 2007).

The aspect is defined as the inclination direction of the maximum rate of change in depth from each cell to its neighbors, the slope inclination ~~Burrough (1986)~~ (Burrough, 1986). The algorithm calculates an aspect value for each cell of a raster and incorporates the respective adjacent cells in both horizontal directions from the center cell (dz/dx and dz/dy) (Table A4).

The BPI describes the relative topographic variability of a central grid cell to a circular annulus with an inner and outer radius,

5   both are manually defined (Table A1) ~~Weiss (2001); Wright et al. (2012)~~ (Weiss, 2001; Wright et al., 2012). For classification a broad BPI (BBPI; large radii) and a fine-scale BPI (FBPI, small radii) are calculated and standardized. Positive values indicate that the central grid cell is elevated with respect to the mean annulus height values, negative values indicate depressions. The BPI is usually subscribed with the applied scale factor (grid cell size $\times$ outer annulus radius).

The Terrain Ruggedness was calculated for the AUV bathymetric data set (Figure A4) using the algorithm for the Vector Terrain Measurement (VRM) of the BTM ~~Sappington et al. (2007)~~ (Sappington et al., 2007). It incorporates slope and aspect heterogeneity of the terrain and is defined as the magnitude of a resultant normalized vector from the decomposed x, y, z compo-

5   nents of the cells and their slope and aspect, normalized to the number of cells in the neighborhood ~~Sappington et al. (2007)~~ (Sappington et al. The Terrain Ruggedness is a unit less measure, ranging from 0 (flat) to 1 (most rugged). All derivative results were displayed and evaluated in ArcGIS 10.2.

A2   Interpretation of Mn-nodule size results

Considering a potential error in correctly detecting nodules by the CoMoNoD algorithm, the application of quantiles of the size distribution allows a more robust interpretation of the data. It is suggested not to use size values of smallest and largest 1% of the quantile calculation, due to the above mentioned error source. The graph in Figure A1 illustrates the quantiles of the calculated sizes of two images, which clearly differ from each other. The graph correctly displays a size difference between both images, indicating more larger nodules for image 29302. This shows that applying CoMoNoD to calculate nodule sizes is

5   reasonable. In this case, the best differentiation exists for the 50% - 75% quantile. Towards larger and smaller size values the two curves approach each other which points towards the detection of similar - none nodule - features in both images. Therefore, the median size values are considered to best represent the Mn-nodule size distribution differences between images/areas. Without ground-truth data from sampling, computed size values should not be used as absolute values for resource assessment. However they can be used to quantify nodule size distributions within seafloor areas and hence to compare variations in nodule

10   distribution and coverage.

Area		Bathymetry	Slope	Aspect	B-BPI	F-BPI	VRM
PA I (Fig. 2)	Grid cell size	110m	110m		110m	110m	
	inner radius				10	10	
	outer radius				100	100	
	scale factor				11000	55000	
Working Area (Fig. 3)	Grid cell size	55m	55m	55m	55m	55m	55m
	inner radius				20	10	
	outer radius				200	50	
	scale factor				11000	2750	
AUV MB (Fig. 24)	Grid cell size	5m	5.5m	5.5m	5.5m	5.5m	5.5m
	inner radius				2		
	outer radius				80		
	scale factor				440		
	Neighborhood (cells)						3x3

Table A1. Metadata of the created maps including raster cell sizes for the considered regions and sub-regions.

Class	Zone	BroadBPI Lower	BroadBPI Upper	FineBPI Lower	FineBPI Upper	Slope Lower	SLope Upper	Depth Lower	Depth Upper
1	seamounts	80							
2	mineable ridges	40	80		100	$0°$	$3°$	-4110m	
3	ridges	40	80		100			-4110m	
4	mineable plateau	-20	40			$0°$	$3°$	-4200m	-4110m
5	elevated plateau	-20	40					-4200m	-4110m
6	flat depression	-70	-10			$0°$	$3°$	-4300m	-4200m
7	depression	-70	-10					-4280m	-4200m
8	mineable deep depression	-160	-70	-230	-10	$0°$	$3°$	-4500m	-4280m
9	deep depression	-160	-70	-230	-10			-4500m	-4280m

Table A2. Classification dictionary with upper and lower bounds for the classification of the PA I area used with the BTM.

Class	Zone	BroadBPI Lower	BroadBPI Upper	FineBPI Lower	FineBPI Upper	Slope Lower	SLope Upper	Depth Lower	Depth Upper
1	mineable elevations	70				0°	3°	-4110m	-4050m
2	un-mineable elevations	70						-4110m	-4050m
3	mineable minor elevations	-20	70			0°	3°	-4130m	-4110m
4	un-mineable minor elevations	-20	70					-4130m	-4110m
5	mineable small scale basins			-130	-40	0°	3°	-4150m	-4130m
6	un-mineable small scale basins			-130	-40			-4150m	-4130m
7	mineable depressions	-80	-20			0°	3°	-4140m	-4125m
8	un-mineable depressions	-80	-20					-4140m	-4125m
9	mineable deep depressions	-280	-80			0°	3°		-4140m
10	un-mineable deep depressions	-280	-80						-4140m

Table A3. Classification dictionary with upper and lower bounds for the classification of the working area used with the BTM.

Bathymetric derivative	ArcGIS Tool	Algorithm	Literature
Slope	Spatial Analyst	slope_degree = $\mathrm{atan}(\sqrt{(dz/dx)^2 + (dz/dy)^2)}) \times 360°/2\pi$	~~Burrough (1986)~~ (Burrough, 1986)
Aspect	BTM	aspect = $\mathrm{atan2}(dz/dy, dz/dx) \times 360°/2\pi$	~~Burrough (1986)~~ (Burrough, 1986)
BPI	BTM	BPI[scalefactor] = int((bathy-focalmean(bathy,annulus,irad,orad))+0.5)	~~Weiss (2001)~~ (Weiss, 2001)
BPI (AUV)	Raster Calculator	BPI[scalefactor] = 'grid'-focalmean('grid',circle,r)	~~Wilson et al. (2007)~~ (Wilson et al., 2007)
BPI_Std	BTM	BPI[scalefactor]_std = int(((BPI<scalefactor>-mean/stddev) × 100)+0.5	~~Weiss (2001)~~ (Weiss, 2001)
VRM	BTM	VRM = $1 - \sqrt{(\sum x)^2 + (\sum y)^2 + (\sum z)^2)}/n$	~~Sappington et al. (2007)~~ (Sappington et al., 20...
Curvature	Spatial Analyst	K = $(\delta^2 Z/\delta S^2)/(1 + \delta Z/\delta S)^2)^{3/2}$	~~Zevenbergen and Thorne (1987)~~ (Zevenbergen and Th...
Plan Curvature	Spatial Analyst	$2 \times (D sin^2\theta + E cos^2\theta - F sin\theta cos\theta)$	~~Zevenbergen and Thorne (1987)~~ (Zevenbergen and Th...
Profile Curvature	Spatial Analyst	$-2 \times (D cos^2\theta + E sin^2\theta - F sin\theta cos\theta)$	~~Zevenbergen and Thorne (1987)~~ (Zevenbergen and Th...

Table A4. Algorithms and ArcGIS Tools applied for the calculation of the bathymetric derivatives.
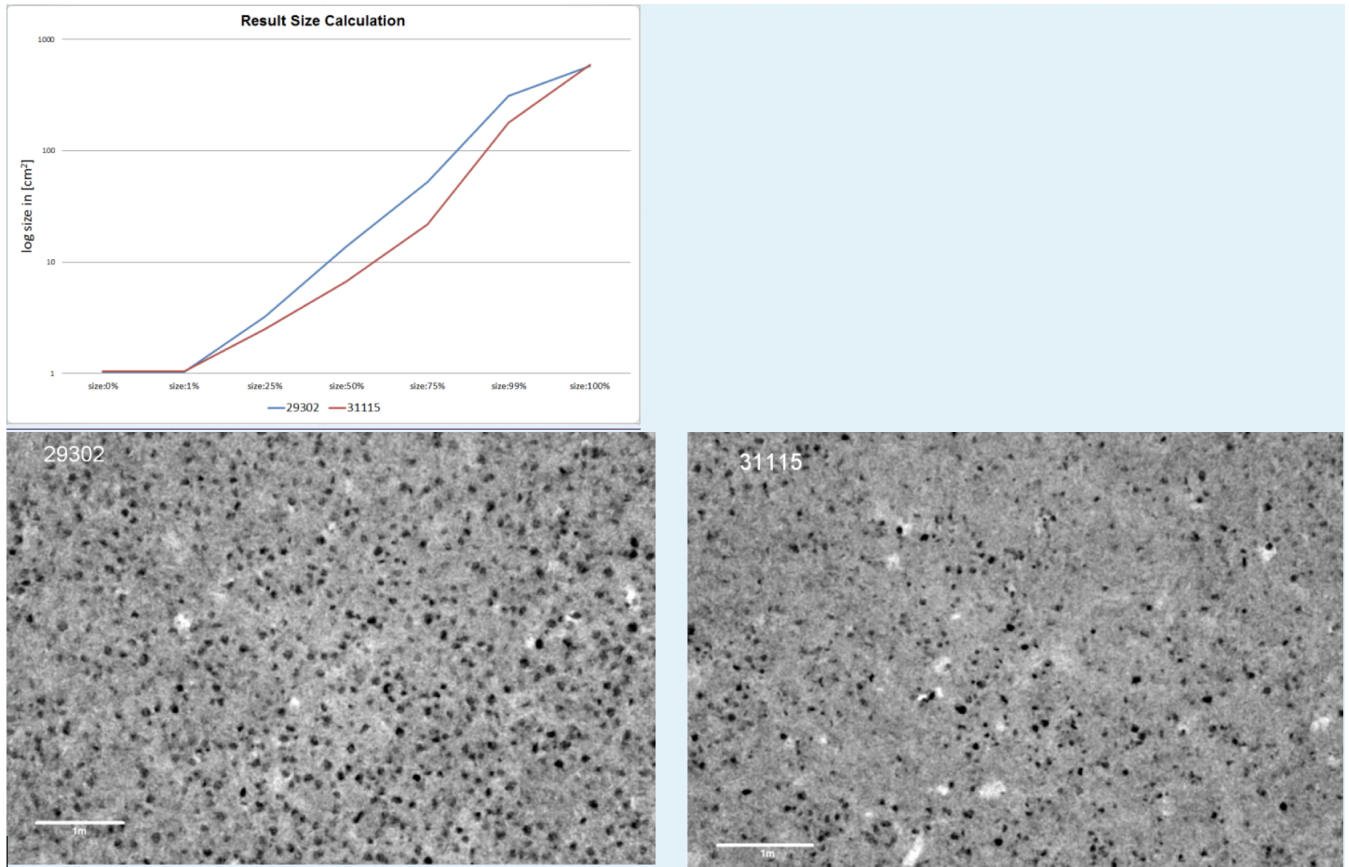
Figure A1. Two example images (bottom) which clearly differ in nodule size and coverage. The graph shows the size distribution as calculated by the CoMoNoD algorithm. The most significant difference is observed in the 75% quantile.

Class	Zone	FineBPI50st Lower	FineBPI50st Upper	Slope Lower [deg]	Slope Upper [deg]	Plan Curvature Lower [radians/m]	Plan Curvature Upper [radians/m]
1	lower coverage	0		0	1.8	-0.02	
2	higher coverage	-200	0	1.5			-0.02
3	no nodules		-200	0	2		-0.1

Table A5. Classification dictionary for the classification of the AUV-mapped study area used with the BTM, to reveal areas of possible lower Mn-nodule coverage.
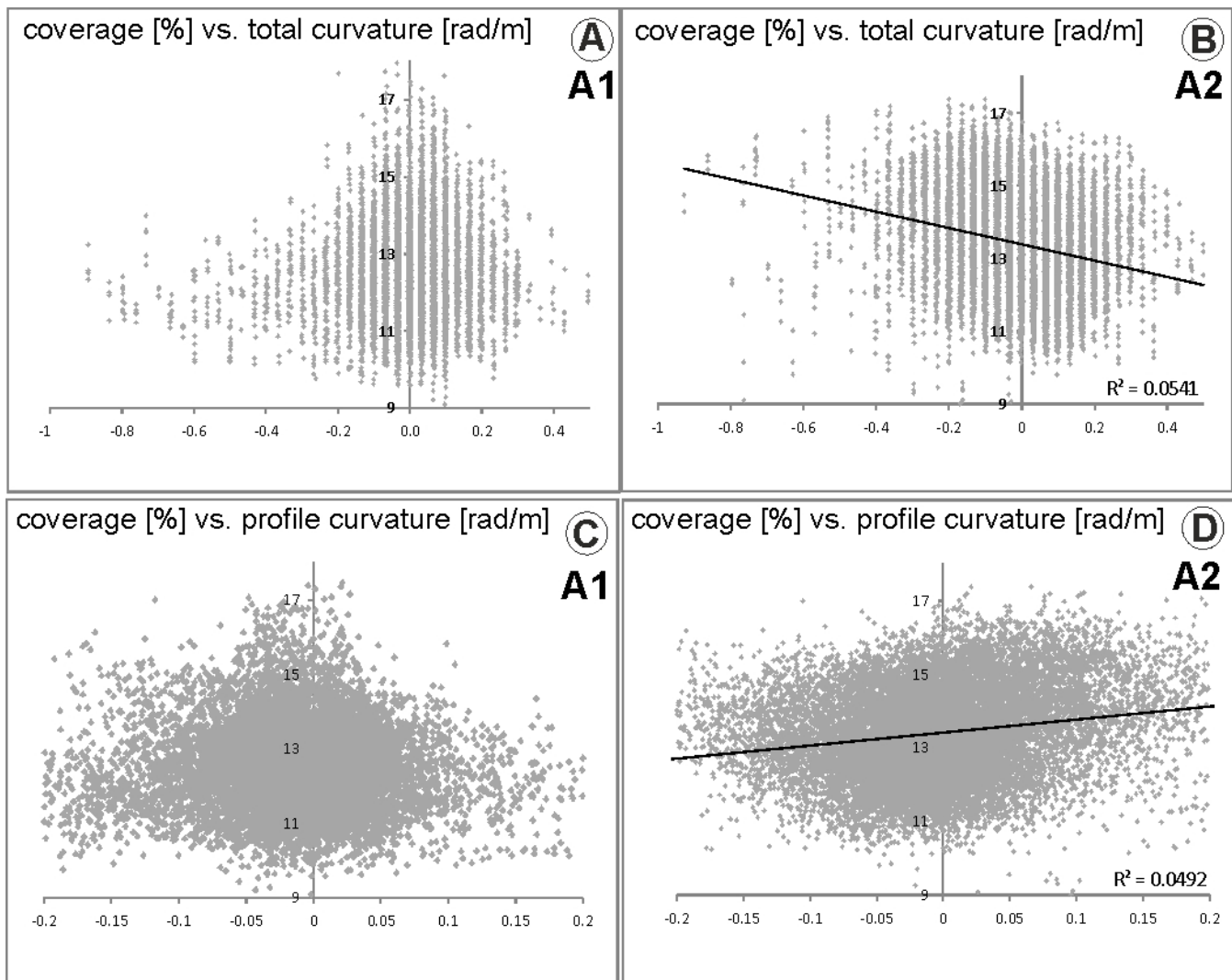
Figure A2. Scatterplots indicating the relation between Mn-nodule coverage and total curvature (A,B) and profile curvature (C,D) in the A1 and A2 sub-areas. Only in area A2 weak correlations could be observed.
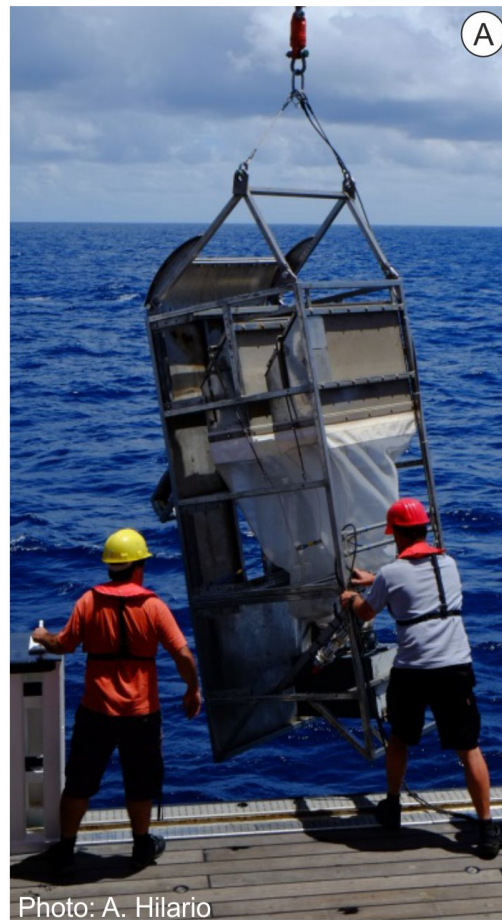
Figure A3. A) The Epibenthic sledge that created the monitored sediment plume (Photo: A. Hilario) ~~Brenke (2005)~~(Brenke, 2005). B) Track created by the EBS at the seafloor, approximately 20 cm deep and 1.5 m wide Photo: ROV Kiel 6000, GEOMAR Helmholtz-Center for Ocean Research Kiel.
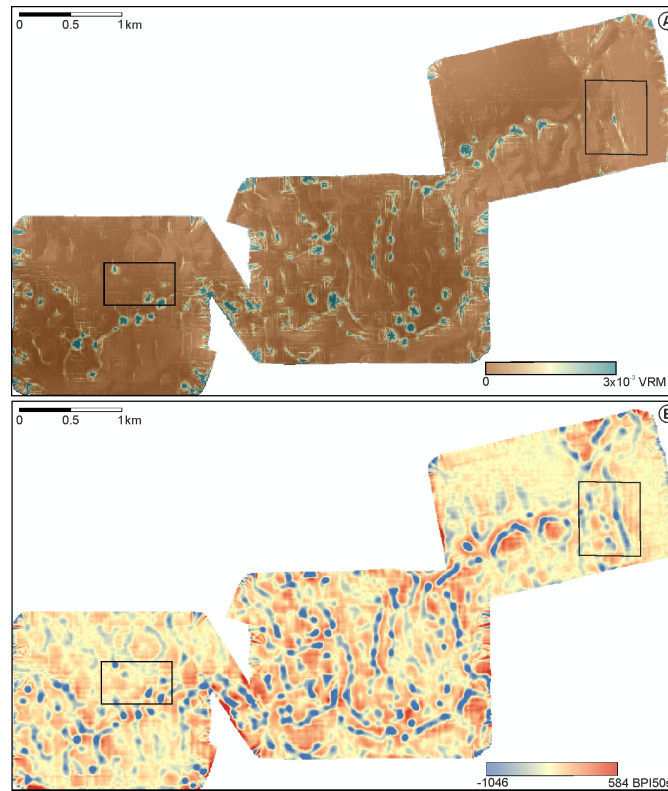
Figure A4. A) Terrain Roughness-indicating map derived from AUV-acquired bathymetry data (calculated with the VRM algorithm ~~Sappington et al. (2007)~~(Sappington et al., 2007). B) BPI50st derived from the AUV-obtained bathymetric data set; the lowest values indicate areas with 'pit-structures' that are observed throughout the entire area.

	Aspect [deg]		Slope [deg]		BPI440st		VRM	
	A1	A2	A1	A2	A1	A2	A1	A2
Mean	163	220	1.28	1.48	-24	-54	9.98E-06	8.12E-06
Median	177	251	0.97	1.28	-13	-61	3.09E-06	3.93E-06
Mode	180	225	0.76	1.50	-6	-97	1.25E-07	1.25E-06
Standard Deviation	64	87	0.93	0.93	68.67	58.98	2.44E-05	1.79E-06
Range	360	361	4.92	4.34	360	316	3.31E-04	3.23E-04
Minimum	0	0	0.03	0.03	-250	-225	0	0
Maximum	360	360	4.95	4.37	110	91	3.31E-04	3.23E-04
Count	10120	16890	10120	16890	10120	16890	10120	16890

Table A6. Statistics summary of the derivatives derived from the AUV-obtained bathymetry for the A1 and A2 survey areas.
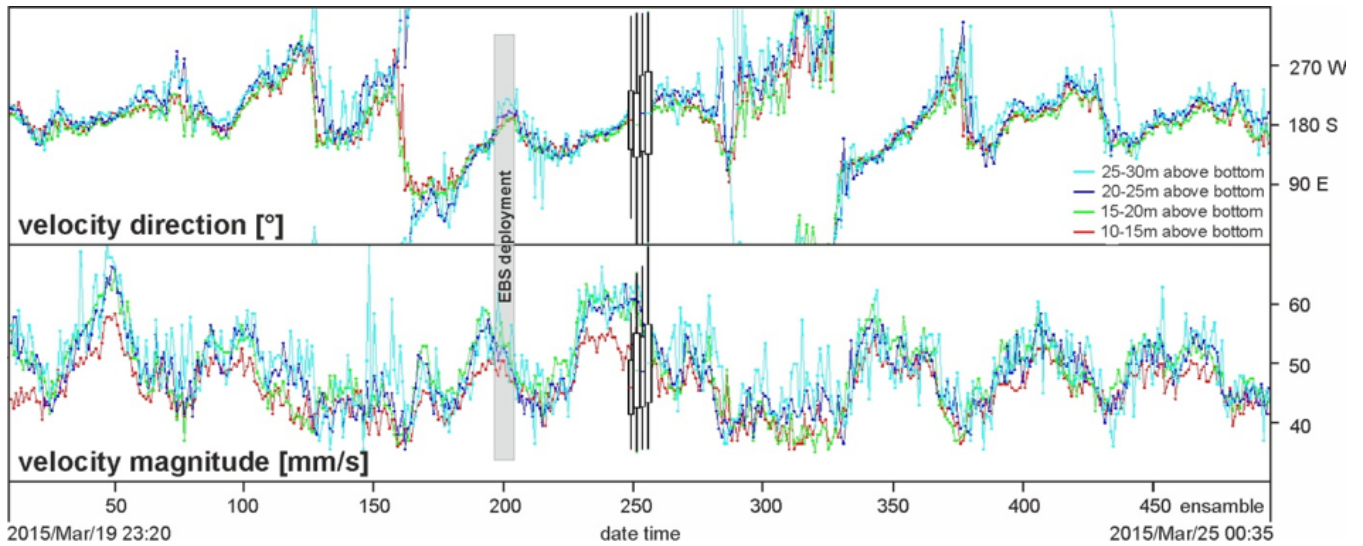
Figure A5. ADCP data obtained by while a DOS lander deployment during SO239 indicating a SSW current flow while the EBS deployment (grey shaded box; ensemble 196 to 204). Box plots show the mean and standard deviation of the time series of the entire deployment. Mean currents between 10 and 30 m above the bottom are towards the south with about 50 mm/s.
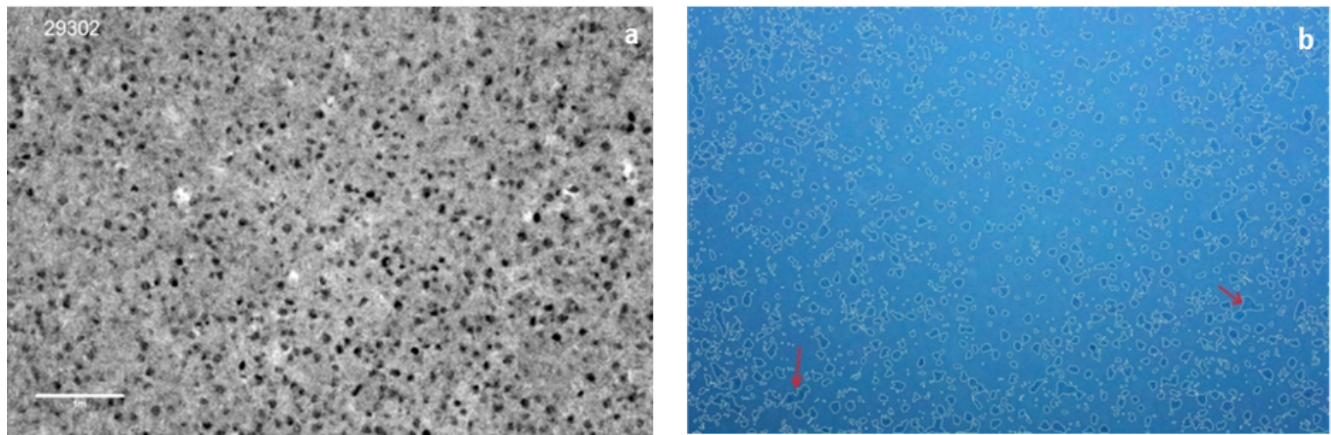

Figure A6. Example for how the program identifies nodules in the image. a) The greyscale image provides higher contrasts for better nodule identification. b) Image showing boundaries of the nodules the program has set for each recognized nodule. Red arrows indicate examples for locations where several nodules are bound together, which leads to larger values in the size calculation. The white scale bar in sub-figure a corresponds to 1m.

References

Barnett, B. and Suzuki, T.: The use of kringing to estimate resedimentation in the JET experiment, in: Proceedings, international symposium
5 on environmental studies for deep-sea mining, pp. 143–151, 1997.

Bluhm, H., Schriever, G., and Thiel, H.: Megabenthic recolonization in an experimentally disturbed abyssal manganese nodule area, Marine georesources & geotechnology, 13, 393–416, 1995.

Boetius, A.: RV SONNE Fahrtbericht/Cruise Report SO242-2 [SO242/2]: JPI OCEANS Ecological Aspects of Deep-Sea Mining, DISCOL Revisited, Guayaquil-Guayaquil (Equador), 28.08.-01.10. 2015, 2015.

10   Brenke, N.: An epibenthic sledge for operations on marine soft bottom and bedrock, Marine Technology Society Journal, 39, 10–21, 2005.

Brockett, T. and Richards, C. Z.: Deepsea mining simulator for environmental impact studies, Sea Technology, 35, 77–82, 1994.

Burns, R.: Observations and measurements during the monitoring of deep ocean manganese nodule mining tests in the North Pacific, March-May 1978, vol. 47, US Department of Commerce, National Oceanic and Atmospheric Administration, Environmental Research Laboratories, 1980.

15   Burrough, P. A.: Principles of geographical information systems for land resources assessment, 1986.

Craig, J. D.: The relationship between bathymetry and ferromanganese deposits in the north equatorial Pacific, Marine Geology, 29, 165–186, 1979.

Edwards, B. D., Dartnell, P., and Chezar, H.: Characterizing benthic substrates of Santa Monica Bay with seafloor photography and multibeam sonar imagery, Marine Environmental Research, 56, 47–66, 2003.

20   Foell, E., Thiel, H., and Schriever, G.: A LONG-TERM, LARGE-SCALE, DISTURBANCE-RECOLONISATION EXPERIMENT IN THE ABYSSAL EASTERN TROPICAL SOUTH PACIFIC OCEAN, 1990.

Frazer, J. and Fisk, M. B.: Geological factors related to characteristics of sea-floor manganese nodule deposits, Deep Sea Research Part A. Oceanographic Research Papers, 28, 1533–1551, 1981.

Fukushima, T. et al.: Overview" Japan Deep-Sea Impact Experiment= JET", in: First ISOPE Ocean Mining Symposium, International Society

25   of Offshore and Polar Engineers, 1995.

Greinert, J.: RV SONNE Fahrtbericht/Cruise Report SO242-1 [SO242/1]: JPI OCEANS Ecological Aspects of Deep-Sea Mining, DISCOL Revisited, Guayaquil-Guayaquil (Equador), 28.07.-25.08. 2015, GEOMAR Reports, 2015.

Greinert, J.: Swath sonar multibeam EM122 bathymetry during SONNE cruise SO239 with links to raw data files., https://doi.org/10.1594/PANGAEA.859456, https://doi.pangaea.de/10.1594/PANGAEA.859456, 2016.

30   Greinert, J., Schoening, T., Köser, K., and Rothenbeck, M.: Seafloor images and raw context data along AUV tracks during SONNE cruises SO239 and SO242/1, https://doi.pangaea.de/10.1594/PANGAEA.882349, 2017.

Halbach, P.: The manganese nodule belt of the Pacific Ocean: Geological environment, nodule formation and mining aspects, Enke, 1988.

Harrington, P.: Formation of pockmarks by pore-water escape, Geo-Marine Letters, 5, 193–197, 1985.

Hovland, M. and Judd, A.: Seabed pockmarks and seepages: impact on geology, biology, and the marine environment, Springer, 1988.

35   Jankowski, J., Malcherek, A., and Zielke, W.: Numerical modeling of suspended sediment due to deep-sea mining, Journal of Geophysical Research: Oceans, 101, 3545–3560, 1996.

Jankowski, J. A. and Zielke, W.: The mesoscale sediment transport due to technical activities in the deep sea, Deep Sea Research Part II: Topical Studies in Oceanography, 48, 3487–3521, 2001.

Jeong, K., Kang, J., and Chough, S.: Sedimentary processes and manganese nodule formation in the Korea Deep Ocean Study (KODOS) area, western part of Clarion-Clipperton fracture zones, northeast equatorial Pacific, Marine Geology, 122, 125–150, 1994.

Jones, A. et al.: Review of benthic impact experiments related to seabed mining, in: Offshore Technology Conference, Offshore Technology

5   Conference, 2000.

Jung, H.-S., Ko, Y.-T., Chi, S.-B., and Moon, J.-W.: Characteristics of seafloor morphology and ferromanganese nodule occurrence in the Korea deep-sea environmental study (KODES) area, NE Equatorial Pacific, Marine georesources & geotechnology, 19, 167–180, 2001.

Kim, J., Hyeong, K., Lee, H.-B., and Ko, Y.-T.: Relationship between polymetallic nodule genesis and sediment distribution in the KODOS (Korea Deep Ocean Study) area, northeastern Pacific, Ocean Science Journal, 47, 197–207, 2012.

10   Kotlinski, R., Stoyanova, V., et al.: Physical, Chemical, And Geological Changes of Marine Environment Caused By the Benthic Impact Experiment At the 10M BIE Site, in: The Eighth International Offshore and Polar Engineering Conference, International Society of Offshore and Polar Engineers, 1998.

Kuhn, T.: Cruise Report SO 240 - FLUM: Low-temperature fluid circulation at seamounts and hydrothermal pits: heat flow regime, impact on biogeochemical processes, and its potential influence on the occurrence and composition of manganese nodules in the equatorial eastern

15   Pacific, https://doi.org/10.2312/cr_so240, 2015.

Kuhn, T. and Rathke, M.: 2017.

Kuhn, T., Rühlemann, C., Wiedicke-Hombach, M., Rutkowsky, J., Wirth, H., Koenig, D., Kleinen, T., and Mathy, T.: Tiefseeförderung von Manganknollen, Schiff & Hafen, 5, 78–83, 2011.

Kuhn, T., Versteegh, G., Villinger, H., Dohrmann, I., Heller, C., Koschinsky, A., Kaul, N., Ritter, S., Wegorzewski, A., and Kasten, S.:

20   Widespread seawater circulation in 18–22 Ma oceanic crust: Impact on heat flow and sediment geochemistry, Geology, 45, 799–802, 2017.

Kwasnitschka, T., Köser, K., Sticklus, J., Rothenbeck, M., Weiß, T., Wenzlaff, E., Schoening, T., Triebe, L., Steinführer, A., Devey, C., et al.: DeepSurveyCam - a deep ocean optical mapping system, Sensors, 16, 164, 2016.

Lavelle, J., Ozturgut, E., Swift, S., and Erickson, B.: Dispersal and resedimentation of the benthic plume from deep-sea mining operations:

25   a model with calibration, Marine Mining, 3, 59–93, 1981.

Markussen, J. M.: Deep Seabed Mining and the Environment: Consequences, Perceptions, and Regulations, Green Globe Yearbook of International Co-operation on Environment and Development, pp. 31–39, 1994.

Martínez Arbizu, P. and Haeckel, M.: RV SONNE Fahrtbericht/cruise report SO239: EcoResponse assessing the ecology, connectivity and resilience of polymetallic nodule field systems, balboa (Panama)–Manzanillo (Mexico,) 11.03.-30.04. 2015, GEOMAR Reports, 2015.

30   Mewes, K., Mogollón, J. M., Picard, A., Rühlemann, C., Kuhn, T., Nöthen, K., and Kasten, S.: Impact of depositional and biogeochemical processes on small scale variations in nodule abundance in the Clarion-Clipperton Fracture Zone, Deep Sea Research Part I: Oceanographic Research Papers, 91, 125–141, 2014.

Oebius, H. U., Becker, H. J., Rolinski, S., and Jankowski, J. A.: Parametrization and evaluation of marine environmental impacts produced by deep-sea manganese nodule mining, Deep Sea Research Part II: Topical Studies in Oceanography, 48, 3453–3467, 2001.

35   Okazaki, M., Tsune, A., et al.: Exploration of Polymetallic Nodule Using AUV in the Central Equatorial Pacific, in: Tenth ISOPE Ocean Mining and Gas Hydrates Symposium, International Society of Offshore and Polar Engineers, 2013.

Ozturgut, E., Lavelle, J., Steffin, O., and Swift, S.: Environmental investigations during manganese nodule mining tests in the north equatorial Pacific in November 1978, 1980.

Park, S. H., Kim, D. H., Kim, C.-W., Park, C. Y., Kang, J. K., et al.: Estimation of coverage and size distribution of manganese nodules based on image processing techniques, in: Second ISOPE Ocean Mining Symposium, International Society of Offshore and Polar Engineers, 1997.

Pattan, J. and Kodagali, V.: Seabed topography and distribution of manganese nodules in the Central Indian Ocean, Mahasagar, 21, 7–12,

5   1988.

Peukert, A.: Correlation of ship- and AUV-based multibeam and side scan sonar analyses with visual AUV- and ROV-based data: Studies for Mn-nodule density quantification and mining-related environmental impact assessments, 2016.

Purser, A., Marcon, Y., Hoving, H.-J. T., Vecchione, M., Piatkowski, U., Eason, D., Bluhm, H., and Boetius, A.: Association of deep-sea incirrate octopods with manganese crusts and nodule fields in the Pacific Ocean, Current Biology, 26, R1268–R1269, 2016.

10 Rühlemann, C., Kuhn, T., Wiedicke, M., Kasten, S., Mewes, K., Picard, A., et al.: Current status of manganese nodule exploration in the German license area, in: Ninth ISOPE Ocean Mining Symposium, International Society of Offshore and Polar Engineers, 2011.

Sappington, J. M., Longshore, K. M., and Thompson, D. B.: Quantifying landscape ruggedness for animal habitat analysis: a case study using bighorn sheep in the Mojave Desert, Journal of wildlife management, 71, 1419–1426, 2007.

Schoening, T.: Results of nodule detection along AUV track SO239_19-1_AUV2 (Abyss_168) during SONNE cruise SO239, 15 https://doi.org/10.1594/PANGAEA.879868, https://doi.org/10.1594/PANGAEA.879868, 2017a.

Schoening, T.: Results of nodule detection along AUV track SO239_28-1_AUV3 (Abyss_169) during SONNE cruise SO239, https://doi.org/10.1594/PANGAEA.879990, https://doi.org/10.1594/PANGAEA.879990, 2017b.

Schoening, T.: Source code for the Compact Morphology-based Nodule Delineation (CoMoNoD) algorithm, https://doi.org/10.1594/PANGAEA.875070, https://doi.org/10.1594/PANGAEA.875070, supplement to: Schoening, Timm; Jones, 20 Daniel O B; Greinert, Jens (2017): Compact-Morphology-based poly-metallic Nodule Delineation. Scientific Reports, 7(1), https://doi.org/10.1038/s41598-017-13335-x, 2017c.

Schoening, T., Kuhn, T., and Nattkemper, T. W.: Estimation of poly-metallic nodule coverage in benthic images, in: Proc. of the 41st Conference of the Underwater Mining Institute (UMI), 2012.

Schoening, T., Kuhn, T., Jones, D. O., Simon-Lledo, E., and Nattkemper, T. W.: Fully automated image segmentation for benthic resource 25 assessment of poly-metallic nodules, Methods in Oceanography, 15, 78–89, 2016.

Schoening, T., Jones, D. O., and Greinert, J.: Compact-morphology-based poly-metallic nodule delineation, Scientific Reports, 7, 13 338, 2017.

Sharma, R.: Indian Deep-sea Environment Experiment (INDEX):: An appraisal, Deep Sea Research Part II: Topical Studies in Oceanography, 48, 3295–3307, 2001.

30 Sharma, R.: Deep-sea mining: Economic, technical, technological, and environmental considerations for sustainable development, Marine Technology Society Journal, 45, 28–41, 2011.

Sharma, R. and Kodagali, V.: Influence of seabed topography on the distribution of manganese nodules and associated features in the Central Indian Basin: A study based on photographic observations, Marine geology, 110, 153–162, 1993.

Sharma, R., Nath, B. N., Parthiban, G., and Sankar, S. J.: Sediment redistribution during simulated benthic disturbance and its implications 35 on deep seabed mining, Deep Sea Research Part II: Topical Studies in Oceanography, 48, 3363–3380, 2001.

Sharma, R., Sankar, S. J., Samanta, S., Sardar, A., and Gracious, D.: Image analysis of seafloor photographs for estimation of deep-sea minerals, Geo-marine letters, 30, 617–626, 2010.

Sharma, R., Khadge, N., and Jai Sankar, S.: Assessing the distribution and abundance of seabed minerals from seafloor photographic data in the Central Indian Ocean Basin, International journal of remote sensing, 34, 1691–1706, 2013.

Shirayama, Y. and Fukushima, T.: Responses of a meiobenthos community to rapid sedimentation, in: Proceedings, international symposium on environmental studies for deep-sea mining, 1997.

Skornyakova, N. and Murdmaa, I.: Local variations in distribution and composition of ferromanganese nodules in the Clarion-Clipperton 5 Nodule Province, Marine Geology, 103, 381–405, 1992.

Thiel, H. and Tiefsee-Umweltschutz, F.: Evaluation of the environmental consequences of polymetallic nodule mining based on the results of the TUSCH Research Association, Deep Sea Research Part II: Topical Studies in Oceanography, 48, 3433–3452, 2001.

Trueblood, D. D., Ozturgut, E., et al.: The benthic impact experiment: A study of the ecological impacts of deep seabed mining on abyssal benthic communities, in: The Seventh International Offshore and Polar Engineering Conference, International Society of Offshore and Polar Engineers, 1997.

Tsune, A., Okazaki, M., et al.: Some Considerations about Image Analysis of Seafloor Photographs for Better Estimation of Parameters of Polymetallic Nodule Distribution, in: The Twenty-fourth International Ocean and Polar Engineering Conference, International Society of Offshore and Polar Engineers, 2014.

Vanreusel, A., Hilario, A., Ribeiro, P. A., Menot, L., and Arbizu, P. M.: Threatened by mining, polymetallic nodules are required to preserve abyssal epifauna, Scientific reports, 6, 26 808, 2016.

von Stackelberg, U. and Beiersdorf, H.: The formation of manganese nodules between the Clarion and Clipperton fracture zones southeast of Hawaii, Marine Geology, 98, 411–423, 1991.

Weiss, A.: Topographic position and landforms analysis, in: Poster presentation, ESRI user conference, San Diego, CA, vol. 200, 2001.

Wessel, P., Smith, W. H., Scharroo, R., Luis, J., and Wobbe, F.: Generic mapping tools: improved version released, Eos, Transactions American Geophysical Union, 94, 409–410, 2013.

Widmann, P., Kuhn, T., and Schulz, H.: Enrichment of mobilizable manganese in deep sea sediments in relation to Mn nodules abundance, in: EGU General Assembly Conference Abstracts, vol. 16, 2014.

Wilson, M. F., O'Connell, B., Brown, C., Guinan, J. C., and Grehan, A. J.: Multiscale terrain analysis of multibeam bathymetry data for habitat mapping on the continental slope, Marine Geodesy, 30, 3–35, 2007.

Wright, D., Pendleton, M., Boulware, J., Walbridge, S., Gerlt, B., Eslinger, D., Sampson, D., and Huntley, E.: ArcGIS Benthic Terrain Modeler (BTM), v. 3.0, Environmental Systems Research Institute, NOAA Coastal Services Center, Massachusetts Office of Coastal Zone Management, esriurl. com/5754, 2012.

Yamada, H., Yamazaki, T., et al.: Japan's ocean test of the nodule mining system, in: The Eighth International Offshore and Polar Engineering Conference, International Society of Offshore and Polar Engineers, 1998.

Yamazaki, T., Kajitani, Y., Barnett, B., Suzuki, T., et al.: Development of image analytical technique for resedimentation induced by nodule mining, in: Second ISOPE Ocean Mining Symposium, International Society of Offshore and Polar Engineers, 1997.

Yamazaki, T., Kajitani, Y., et al.: Deep-sea environment and impact experiment to it, in: The Ninth International Offshore and Polar Engineering Conference, International Society of Offshore and Polar Engineers, 1999.

You, Z.-J.: The effect of suspended sediment concentration on the settling velocity of cohesive sediment in quiescent water, Ocean Engineering, 31, 1955–1965, 2004.

Zevenbergen, L. W. and Thorne, C. R.: Quantitative analysis of land surface topography, Earth surface processes and landforms, 12, 47–56, 1987.